

A Scalable Belief Propagation Algorithm for Radio Signal Based SLAM

Erik Leitinger, *Member, IEEE*, Florian Meyer, *Member, IEEE*, Franz Hlawatsch, *Fellow, IEEE*, Klaus Witrisal, *Member, IEEE*, Fredrik Tufvesson, *Fellow, IEEE*, and Moe Z. Win, *Fellow, IEEE*

Abstract

We present a simultaneous localization and mapping (SLAM) algorithm that is based on radio signals and the association of specular multipath components (MPCs) with geometric features. Especially in indoor scenarios, localization from radio signals is challenging due to diffuse multipath propagation and the unknown MPC-feature association. In our approach, specular reflections at flat surfaces (e.g., walls) are described in terms of virtual anchors (VAs). The positions of these VAs are unknown and possibly time-varying. We develop a Bayesian model of the SLAM problem including the unknown MPC-VA association. We represent this model by a factor graph, which enables the use of the belief propagation (BP) scheme for efficient marginalization of the joint posterior distribution. The resulting BP-based SLAM algorithm detects the VAs and estimates the time-varying position of the mobile agent and the possibly time-varying positions of the VAs, thereby leveraging the MPCs in the radio signal for improved accuracy and robustness of agent localization. A core aspect of the algorithm is BP-based probabilistic MPC-VA association. Moreover, for improved initialization of new VA positions, the states of unobserved potential VAs are modeled as a random finite set and propagated in time by means of a “zero-measurement” probability hypothesis density filter. The proposed BP-based SLAM algorithm has a low computational complexity and scales well in all relevant system parameters. Experimental results using both synthetically generated measurements and real ultra-wideband radio signals demonstrate the excellent performance of the algorithm in challenging indoor environments.

Index Terms

Simultaneous localization and mapping, SLAM, multipath channel, data association, factor graph, message passing, sum-product algorithm.

E. Leitinger and F. Tufvesson are with the Department of Electrical and Information Technology, Lund University, Lund, Sweden (e-mail: {erik.leitinger, fredrik.tufvesson}@eit.lth.se). F. Meyer and M. Win are with the Laboratory for Information and Decision Systems, Massachusetts Institute of Technology, Cambridge, MA, USA (e-mail: {fmeyer,moewin}@mit.edu). F. Hlawatsch is with the Institute of Telecommunications, TU Wien, Vienna, Austria and with Brno University of Technology, Brno, Czech Republic (e-mail: franz.hlawatsch@tuwien.ac.at). K. Witrisal is with the Laboratory of Signal Processing and Speech Communication, Graz University of Technology, Graz, Austria, (e-mail: witrisal@tugraz.at). This work was supported in part by the Austrian Science Fund (FWF) under grants J 4027, J 3886, and P27370-N30, by the U.S. Department of Commerce, National Institute of Standards and Technology under Grant 70NANB17H17, and by the Czech Science Foundation (GAČR) under grant 17-19638S. Parts of this paper were presented at IEEE ICC, ANLN Workshop 2017, Paris, France, June 2017.

I. INTRODUCTION

The purpose of simultaneous localization and mapping (SLAM) [1] is to estimate the time-varying pose of a mobile agent—which includes the agent’s position—and a map of the surrounding environment from measurements provided by one or multiple sensors. SLAM has attracted strong interest in robotics research for many years. Other fields that rely on accurate localization and environment mapping include autonomous driving [2], location-aware communication [3], and robust indoor localization [4]–[7]. This paper presents a SLAM algorithm for robust indoor localization based on radio signals. The radio signals are transmitted from a mobile agent to base stations, called physical anchors (PAs). Multipath components (MPCs) due to specular reflections at flat surfaces are modeled by virtual anchors (VAs), which are mirror images of the PAs. Our algorithm is able to detect the VAs and to accurately estimate the VA positions jointly with the time-varying position of the mobile agent.

A. Feature-based SLAM

The proposed algorithm follows the feature-based approach to SLAM [1], [8], [9]. The map is represented by an unknown number of *features* with unknown spatial positions, whose states are estimated in a sequential (i.e., time-recursive) fashion. Features are parametric descriptions of the physical environment such as flat surfaces, edges, corners, points, or circles. In our model, the features are given by the PAs and VAs. Prominent feature-based SLAM algorithms are extended Kalman filter SLAM (EKF-SLAM) [8], Rao-Blackwellized SLAM (dubbed FastSLAM) [1], variational-inference-based SLAM [10], [11], and set-based SLAM [9], [12], [13]. Recently, feature-based SLAM methods that exploit position-related information in radio signals have been introduced [14]–[16]. Most of these methods operate on estimated parameters related to MPCs, such as distances (which are proportional to delays), angles-of-arrival (AoAs), or angles-of-departure (AoDs) [17]–[21]. These parameter estimates are calculated from the signal in a preprocessing stage and are considered as “measurements” by the SLAM method. As in other feature-based SLAM methods, an important aspect of radio signal-based SLAM is the *data association* (DA) between these measurements and the PAs or VAs.

Feature-based SLAM is closely related to the multitarget tracking (MTT) problem, and consequently MTT methods have been adapted to feature-based SLAM [9], [12], [22]. MTT methods that are applicable to SLAM include the joint probabilistic DA (JPDA) filter [23] and the joint integrated probabilistic DA (JIPDA) filter [24]. An approach similar to the JIPDA filter is taken

by the methods presented in [25], [26], which determine a track quality measure and use an additional random finite set (RFS)-based probability hypothesis density (PHD) filter [27] to initialize new objects; these methods are suited to an unknown and time-varying number of objects. More recently, the use of the belief propagation (BP) message passing scheme [28], [29] was introduced for probabilistic DA within MTT in [30] and for multisensor MTT in [31]–[33]. In particular, the BP algorithms in [31]–[33] are based on a factor graph representation of the multisensor MTT problem and have a computational complexity that scales only quadratically with the number of objects (targets) and linearly with the number of sensors. MTT methods that are based on RFSs and embed a BP algorithm for probabilistic DA were presented in [34], [35].

B. Contributions and Organization of the Paper

Here, we propose a BP algorithm for SLAM based on radio signals. The algorithm jointly performs probabilistic DA and sequential Bayesian estimation of the state of a mobile agent and the states of “potential features” (PFs) characterizing the environment. Each PF state is augmented by a binary existence variable and associated with a *probability of existence*, which is also estimated. The proposed SLAM algorithm is inspired by the BP algorithms for multisensor MTT presented in [31]–[33]. Probabilistic DA and state estimation are performed by running BP on a factor graph [28], [29] representing the statistical structure of the SLAM detection-estimation problem. The BP approach leverages conditional statistical independencies to achieve low complexity and high scalability. Indeed, the complexity of the SLAM algorithm scales only quadratically with the numbers of features and measurements and linearly with the number of PAs. A major reason for this scalability is the integration of a BP-based probabilistic DA scheme involving both feature-oriented and measurement-oriented association variables [30], [31] in the overall BP-based algorithm. The proposed algorithm distinguishes between *legacy PFs*, which correspond to features that already generated measurements in the past, and *new PFs*, which correspond to features that generate measurements for the first time. The parameters required to initialize new PFs are modeled explicitly by means of an *undetected feature* state and inferred using a “zero-measurement” PHD filter, which was introduced in the context of MTT in [26], [34]. To the best of our knowledge, the proposed algorithm—along with a preliminary version presented in [22]—is the first BP algorithm for feature-based SLAM with probabilistic DA.

Key innovative contributions of this paper include the following:

- We develop a BP algorithm for feature-based SLAM with probabilistic DA that uses MPC parameters extracted from radio signals as input measurements. The algorithm takes into account that the number of features is unknown and possibly time-varying, and it scales well with all relevant system parameters.
- We consider the states of *new PFs* and an *undetected feature* state. The intensity function of the undetected feature state is tracked by a zero-measurement PHD filter [26]. The estimated intensity function is used to determine the initial distribution of new PFs.
- We evaluate the performance of the proposed algorithm on synthetic and real data. Our results show that the algorithm is able to estimate the position of the mobile agent and a possibly time-varying feature map with high accuracy and robustness.

This paper advances over our conference paper [22] in that it replaces the heuristic used therein for determining the initial distribution of new PFs by an improved Bayesian scheme. The factor graph and BP algorithm of [22] are extended by the introduction of new PFs, i.e., features that generate measurements for the first time. For simplicity of exposition, we assume in this work that the probabilities with which the preliminary signal analysis stage (producing measurements) detects features in the radio signals are known; however, an adaptive extension to unknown and time-varying detection probabilities can be obtained along the lines of [22].

The remainder of this paper is organized as follows. Section II considers the received radio signals and the MPC parameters. Section III describes the system model and provides a statistical formulation of the SLAM problem. The posterior distribution of all states and the corresponding factor graph are derived in Section IV. In Section V, the proposed BP algorithm is described. Section VI discusses the determination of the initial distribution of new PFs. The results of numerical experiments are reported in Section VII. Section VIII concludes the paper.

II. RADIO SIGNAL AND MPC PARAMETERS

Radio signal based SLAM [4], [14]–[16] exploits position-related information in MPCs [36]. Specular MPC parameters estimated from the received radio signals are associated with “geometrically expected” parameters, such as distances (corresponding to delays), AoAs, and AoDs. These “geometrically expected” parameters are modeled in terms of the position of the mobile agent and the positions of the PAs or of the corresponding VAs. The VA positions are mirror images of the PA positions. These mirror images are induced by reflections at flat surfaces (typically walls), and thus depend on the surrounding environment (floor plan). An example is

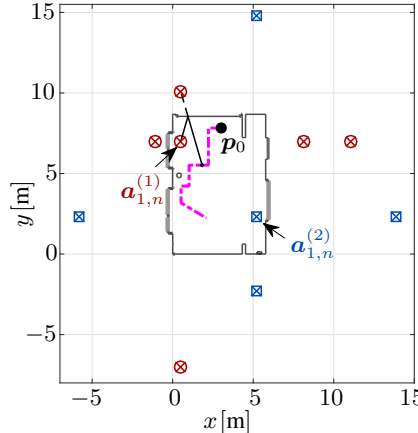


Fig. 1: Example of an environment map (floor plan). The PAs at fixed positions $\mathbf{a}_{1,n}^{(1)}$ (PA 1) and $\mathbf{a}_{1,n}^{(2)}$ (PA 2) are indicated by, respectively, a red circle-cross and a blue square-cross within the floor plan. The magenta dashed-dotted line represents the trajectory of the mobile agent. The starting position of the mobile agent, p_0 , is indicated by a black bullet. The red circle-crosses and blue square-crosses outside the floor plan indicate some of the geometrically expected VAs corresponding to PA 1 and PA 2, respectively.

shown in Fig. 1, which depicts two PAs and some of the corresponding VAs. The VA positions are unknown because the floor plan is unknown.

We consider a mobile agent with unknown time-varying position $\mathbf{p}_n \in \mathbb{R}^2$ and J PAs with possibly unknown time-varying positions $\mathbf{a}_{1,n}^{(j)} \in \mathbb{R}^2$, $j = 1, \dots, J$, where J is assumed to be known. Associated with the j th PA, there are $L_n^{(j)} - 1$ VAs at unknown and possibly time-varying positions $\mathbf{a}_{l,n}^{(j)} \in \mathbb{R}^2$, $l = 2, \dots, L_n^{(j)}$. The PAs and VAs will also be referred to as *features*. The number of features, $L_n^{(j)}$, is unknown and time-varying, and it depends on the agent position \mathbf{p}_n . We note that the PA and VA positions are allowed to be time-varying for the sake of generality; in an indoor scenario, they are typically static. In each discrete time slot n , depending on the radio transmission protocol, the j th PA transmits or receives a baseband radio signal $s^{(j)}(t)$ or $s(t)$, respectively. If the PAs act as receivers, they receive one common signal $s(t)$ from the mobile agent. If the PAs act as transmitters, their signals $s^{(j)}(t)$ are received by the mobile agent, where they can be separated based on a multiple access scheme such as CDMA [37, Chapter 16]. In the following, we consider the case where the mobile agent transmits $s(t)$ and the PAs act as receivers. The signal received by the j th PA is modeled as [36]

$$r_n^{(j)}(t) = \sum_{l=1}^{L_n^{(j)}} \alpha_{l,n}^{(j)} s(t - \tau_{l,n}^{(j)}) + d_n^{(j)}(t) + w(t). \quad (1)$$

Here, the first term on the right-hand side describes the contribution of $L_n^{(j)}$ specular MPCs with complex amplitudes $\alpha_{l,n}^{(j)}$ and delays $\tau_{l,n}^{(j)}$, where $l \in \mathcal{L}_n^{(j)} \triangleq \{1, \dots, L_n^{(j)}\}$. The specular MPCs

potentially correspond to features (PA or VA). The delays $\tau_{l,n}^{(j)}$ are proportional to the ranges (distances) between the agent and the j th PA (for $l = 1$) or between the agent and the VAs associated with the j th PA (for $l \in \{2, \dots, L_n^{(j)}\}$). That is, $\tau_{l,n}^{(j)} = \|\mathbf{p}_n - \mathbf{a}_{l,n}^{(j)}\|/c$, where c is the speed of light. The second term in (1), $d_n^{(j)}(t)$, represents the diffuse multipath, which shares the same spectrum as $s(t)$ and interferes with the position-related MPC term. The third and last term in (1), $w(t)$, is additive white Gaussian noise.

We note that expression (1) presupposes a common time reference at the mobile agent and at the PAs, i.e., a synchronized system; however, the proposed SLAM algorithm can be extended to an unsynchronized system along the lines discussed in [15]. Furthermore, expression (1), as well as the proposed algorithm, can also be extended to the case where the MPC parameters include AoAs and/or AoDs in addition to the delays $\tau_{l,n}^{(j)}$.

In each time slot n and for each PA $j \in \{1, \dots, J\}$, the MPC parameters (e.g., delays, AoAs, and AoDs) are estimated from the radio signals $r_n^{(j)}(t)$ using a snapshot-based [17], [18], [20], [21] or state space-based [19], [38] parametric radio channel estimator. This results in $M_n^{(j)}$ estimates of MPC parameters along with estimates of the corresponding complex amplitudes $\alpha_{m,n}^{(j)}$, with $m \in \mathcal{M}_n^{(j)} \triangleq \{1, \dots, M_n^{(j)}\}$, for each PA $j \in \{1, \dots, J\}$. The set of estimated MPC parameters $\mathcal{M}_n^{(j)}$ is related to the set of specular MPCs $\mathcal{L}_n^{(j)}$ as follows. It is possible that some specular MPCs are not “detected” by the radio channel estimator and thus do not produce an MPC parameter estimate, and it is also possible that some estimates do not correspond to specular MPCs. Accordingly, $M_n^{(j)} = |\mathcal{M}_n^{(j)}|$ may be smaller than, equal to, or larger than $L_n^{(j)} = |\mathcal{L}_n^{(j)}|$. (Here, $|\cdot|$ denotes the cardinality of a set.) Note also that $M_n^{(j)}$ depends on the agent position \mathbf{p}_n , on the surrounding environment, and on the channel parameter estimation algorithm. The amplitude estimates are used to determine estimates of the MPC parameter variances $\sigma_{m,n}^{(j)2}$, if such variance estimates are not provided by the channel estimator (cf. Section VII-C). We denote by $\mathbf{z}_{m,n}^{(j)}$ with $m \in \mathcal{M}_n^{(j)}$ the m th MPC parameter estimate of PA j . The stacked vectors $\mathbf{z}_n^{(j)} \triangleq [\mathbf{z}_{1,n}^{(j)\top} \cdots \mathbf{z}_{M_n^{(j)},n}^{(j)\top}]^\top$ are used as noisy “measurements” by the proposed SLAM algorithm.

III. SYSTEM MODEL AND STATISTICAL FORMULATION

A. Agent State and PF States

The state of the mobile agent at time n is defined as $\mathbf{x}_n \triangleq [\mathbf{p}_n^\top \mathbf{v}_n^\top]^\top$, where \mathbf{v}_n is the agent’s velocity. For each PA $j \in \{1, \dots, J\}$, there are $K_n^{(j)}$ PFs. Thus, the PFs will be indexed by the tuple (j, k) , where $j \in \{1, \dots, J\}$ and $k \in \mathcal{K}_n^{(j)} \triangleq \{1, \dots, K_n^{(j)}\}$. Whereas the number of PAs J is

known, the number of PFs $K_n^{(j)}$ (for PA j) is unknown and random. The existence of the (j, k) th PF as an actual *feature* is indicated by the binary existence variable $r_{k,n}^{(j)} \in \{0, 1\}$, where $r_{k,n}^{(j)} = 0$ ($r_{k,n}^{(j)} = 1$) means that the PF does not exist (exists) at time n . The state of PF (j, k) is the PF's position $\mathbf{a}_{k,n}^{(j)}$, and the *augmented state* of a PF (j, k) is defined as $\mathbf{y}_{k,n}^{(j)} \triangleq [\mathbf{a}_{k,n}^{(j)\top} \ r_{k,n}^{(j)}]^\top$ [31]. We also define the stacked vectors $\mathbf{y}_n^{(j)} \triangleq [\mathbf{y}_{1,n}^{(j)\top} \cdots \mathbf{y}_{K_n^{(j)},n}^{(j)\top}]^\top$ and $\mathbf{y}_n \triangleq [\mathbf{y}_n^{(1)\top} \cdots \mathbf{y}_n^{(J)\top}]^\top$. It will be convenient to formally consider states $\mathbf{a}_{k,n}^{(j)}$ also for the nonexisting PFs (case $r_{k,n}^{(j)} = 0$); however, the values of these states are obviously irrelevant. Therefore, all probability density functions (pdfs) defined for an augmented state, $f(\mathbf{y}_{k,n}^{(j)}) = f(\mathbf{a}_{k,n}^{(j)}, r_{k,n}^{(j)})$, are such that for $r_{k,n}^{(j)} = 0$, $f(\mathbf{a}_{k,n}^{(j)}, 0) = f_{k,n}^{(j)} f_D(\mathbf{a}_{k,n}^{(j)})$, where $f_D(\mathbf{a}_{k,n}^{(j)})$ is an arbitrary “dummy pdf” and $f_{k,n}^{(j)} \geq 0$ can be interpreted as the probability of nonexistence of the PF [31]. Furthermore, for BP messages defined for an augmented state, $\phi(\mathbf{y}_{k,n}^{(j)}) = \phi(\mathbf{a}_{k,n}^{(j)}, r_{k,n}^{(j)})$, we have $\phi(\mathbf{a}_{k,n}^{(j)}, 0) = \phi_{k,n}^{(j)}$ (note that these BP messages are not pdfs and thus are not required to integrate to 1).

At any time n , each PF is either a *legacy PF*, which was already established in the past, or a *new PF*. The augmented states of legacy PFs and new PFs for PA j will be denoted by $\tilde{\mathbf{y}}_{k,n}^{(j)} \triangleq [\tilde{\mathbf{a}}_{k,n}^{(j)\top} \ \tilde{r}_{k,n}^{(j)}]^\top$, $k \in \mathcal{K}_{n-1}^{(j)}$ and $\check{\mathbf{y}}_{m,n}^{(j)} \triangleq [\check{\mathbf{a}}_{m,n}^{(j)\top} \ \check{r}_{m,n}^{(j)}]^\top$, $m \in \mathcal{M}_n^{(j)}$, respectively. Thus, the number of new PFs equals the number of measurements, $M_n^{(j)}$. The set and number of legacy PFs are updated according to¹

$$\mathcal{K}_n^{(j)} = \mathcal{K}_{n-1}^{(j)} \cup \mathcal{M}_n^{(j)}, \quad K_n^{(j)} = K_{n-1}^{(j)} + M_n^{(j)}, \quad (2)$$

where the first relation is understood to include a suitable reindexing of the elements of $\mathcal{M}_n^{(j)}$. We also define the following state-related vectors. For the legacy PFs for PA j , $\tilde{\mathbf{a}}_n^{(j)} \triangleq [\tilde{\mathbf{a}}_{1,n}^{(j)\top} \cdots \tilde{\mathbf{a}}_{K_{n-1}^{(j)},n}^{(j)\top}]^\top$, $\tilde{r}_n^{(j)} \triangleq [\tilde{r}_{1,n}^{(j)} \cdots \tilde{r}_{K_{n-1}^{(j)},n}^{(j)}]^\top$, and $\tilde{\mathbf{y}}_n^{(j)} \triangleq [\tilde{\mathbf{y}}_{1,n}^{(j)\top} \cdots \tilde{\mathbf{y}}_{K_{n-1}^{(j)},n}^{(j)\top}]^\top$. For the new PFs for PA j , $\check{\mathbf{a}}_n^{(j)} \triangleq [\check{\mathbf{a}}_{1,n}^{(j)\top} \cdots \check{\mathbf{a}}_{M_n^{(j)},n}^{(j)\top}]^\top$, $\check{r}_n^{(j)} \triangleq [\check{r}_{1,n}^{(j)} \cdots \check{r}_{M_n^{(j)},n}^{(j)}]^\top$, and $\check{\mathbf{y}}_n^{(j)} \triangleq [\check{\mathbf{y}}_{1,n}^{(j)\top} \cdots \check{\mathbf{y}}_{M_n^{(j)},n}^{(j)\top}]^\top$. For the combination of legacy PFs and new PFs for PA j , $\mathbf{y}_n^{(j)} \triangleq [\tilde{\mathbf{y}}_n^{(j)\top} \ \check{\mathbf{y}}_n^{(j)\top}]^\top$; note that the vector entries (subvectors) of $\mathbf{y}_n^{(j)}$ are given by $\mathbf{y}_{k,n}^{(j)}$ for $k \in \mathcal{K}_n^{(j)} = \mathcal{K}_{n-1}^{(j)} \cup \mathcal{M}_n^{(j)}$. For all the legacy PFs, $\tilde{\mathbf{y}}_n \triangleq [\tilde{\mathbf{y}}_n^{(1)\top} \cdots \tilde{\mathbf{y}}_n^{(J)\top}]^\top$, and for all the new PFs, $\check{\mathbf{y}}_n \triangleq [\check{\mathbf{y}}_n^{(1)\top} \cdots \check{\mathbf{y}}_n^{(J)\top}]^\top$.

The number of new PFs at time n is known only after the current measurements have been observed. Features that are observed for the first time will be referred to as *newly detected features*. Before the current measurements are observed, only prior information about the newly

¹In a practical implementation, as will be explained in Section V-A, the set of PFs is pruned at each time n , and therefore the number of PFs does not actually grow by $M_n^{(j)}$.

detected features is available (as discussed in Section VI-B). After the current measurements are observed, newly detected features are represented by new PFs.

B. Association Vectors

For each PA j , the measurements (MPC parameter estimates) $\mathbf{z}_{m,n}^{(j)}$, $m \in \mathcal{M}_n^{(j)}$ described in Section II are subject to a measurement origin uncertainty, also known as DA uncertainty. That is, it is not known which measurement $\mathbf{z}_{m,n}^{(j)}$ is associated with which PF $k \in \mathcal{K}_n^{(j)}$, or if a measurement $\mathbf{z}_{m,n}^{(j)}$ did not originate from any PF (this is known as a *false alarm* or *clutter*), or if a PF did not give rise to any measurement (this is known as a *missed detection*). The probability that a PF is “detected” in the sense that it generates a measurement $\mathbf{z}_{m,n}^{(j)}$ in the MPC parameter estimation stage is denoted by $P_d^{(j)}(\mathbf{x}_n, \mathbf{a}_{k,n}^{(j)})$. The distribution of false alarm measurements, described by the pdf $f_{\text{FA}}(\mathbf{z}_{m,n}^{(j)})$, is assumed to be known. Following [23], we will use the assumption that at any time n , each PF can generate at most one measurement, and each measurement can be generated by at most one PF.

For each PA j , the associations between the measurements $m \in \mathcal{M}_n^{(j)}$ and the legacy PF states (j, k) , $k \in \mathcal{K}_{n-1}^{(j)}$ at time n can be described by the $K_{n-1}^{(j)}$ -dimensional *feature-oriented DA vector* $\mathbf{c}_n^{(j)} = [c_{1,n}^{(j)} \cdots c_{K_{n-1}^{(j)},n}^{(j)}]^T$ with entries

$$c_{k,n}^{(j)} \triangleq \begin{cases} m \in \mathcal{M}_n^{(j)}, & \text{if at time } n, \text{ legacy PF } (j, k) \text{ generates measurement } \mathbf{z}_{m,n}^{(j)}; \\ 0, & \text{if at time } n, \text{ legacy PF } (j, k) \text{ does not generate any measurement.} \end{cases} \quad (3)$$

We also define $\mathbf{c}_n \triangleq [\mathbf{c}_n^{(1)T} \cdots \mathbf{c}_n^{(J)T}]^T$. In addition, following [30], [31], we consider the $M_n^{(j)}$ -dimensional *measurement-oriented DA vector* $\mathbf{b}_n^{(j)} = [b_{1,n}^{(j)} \cdots b_{M_n^{(j)},n}^{(j)}]^T$ with entries

$$b_{m,n}^{(j)} \triangleq \begin{cases} k \in \mathcal{K}_{n-1}^{(j)}, & \text{if measurement } \mathbf{z}_{m,n}^{(j)} \text{ is generated by legacy PF } (j, k); \\ 0, & \text{if measurement } \mathbf{z}_{m,n}^{(j)} \text{ is not generated by any legacy PF.} \end{cases} \quad (4)$$

We also define $\mathbf{b}_n \triangleq [\mathbf{b}_n^{(1)T} \cdots \mathbf{b}_n^{(J)T}]^T$. The two DA vectors \mathbf{c}_n and \mathbf{b}_n are unknown and modeled as random. They are equivalent since one can be determined from the other. The redundant formulation of DA uncertainty in terms of both \mathbf{c}_n and \mathbf{b}_n is key to obtaining the scalability properties of the BP algorithm to be presented in Section V-B. Furthermore, as will be discussed in Section IV, it facilitates the establishment of a factor graph for the problem of jointly inferring the agent state and the states of the legacy PFs and new PFs.

C. State Evolution

The agent state \mathbf{x}_n and the augmented states of the legacy PFs, $\tilde{\mathbf{y}}_{k,n}^{(j)}$, are assumed to evolve independently according to Markovian state dynamics, i.e.,

$$f(\mathbf{x}_n, \tilde{\mathbf{y}}_n | \mathbf{x}_{n-1}, \mathbf{y}_{n-1}) = f(\mathbf{x}_n | \mathbf{x}_{n-1}) \prod_{j=1}^J \prod_{k=1}^{K_{n-1}^{(j)}} f(\tilde{\mathbf{y}}_{k,n}^{(j)} | \mathbf{y}_{k,n-1}^{(j)}), \quad (5)$$

where $f(\mathbf{x}_n | \mathbf{x}_{n-1})$ and $f(\tilde{\mathbf{y}}_{k,n}^{(j)} | \mathbf{y}_{k,n-1}^{(j)})$ are the state-transition pdfs of the agent and of legacy PF (j, k) , respectively. Note that $\tilde{\mathbf{y}}_{k,n}^{(j)}$ depends on both $\mathbf{y}_{k,n-1}^{(j)}$ and $\check{\mathbf{y}}_{m,n-1}^{(j)}$.

If PF (j, k) existed at time $n-1$, i.e., $r_{k,n-1}^{(j)} = 1$, it either dies, i.e., $\tilde{r}_{k,n}^{(j)} = 0$, or survives, i.e., $\tilde{r}_{k,n}^{(j)} = 1$; in the latter case, it becomes a legacy PF at time n . The probability of survival is denoted by P_s . If the PF survives, its new state $\tilde{\mathbf{a}}_{k,n}^{(j)}$ is distributed according to the state-transition pdf $f(\tilde{\mathbf{a}}_{k,n}^{(j)} | \mathbf{a}_{k,n-1}^{(j)})$. Therefore, $f(\tilde{\mathbf{y}}_{k,n}^{(j)} | \mathbf{y}_{k,n-1}^{(j)}) = f(\tilde{\mathbf{a}}_{k,n}^{(j)}, \tilde{r}_{k,n}^{(j)} | \mathbf{a}_{k,n-1}^{(j)}, r_{k,n-1}^{(j)})$ in (5) is given for $r_{k,n-1}^{(j)} = 1$ by

$$f(\tilde{\mathbf{a}}_{k,n}^{(j)}, \tilde{r}_{k,n}^{(j)} | \mathbf{a}_{k,n-1}^{(j)}, r_{k,n-1}^{(j)} = 1) = \begin{cases} (1 - P_s) f_D(\tilde{\mathbf{a}}_{k,n}^{(j)}), & \tilde{r}_{k,n}^{(j)} = 0 \\ P_s f(\tilde{\mathbf{a}}_{k,n}^{(j)} | \mathbf{a}_{k,n-1}^{(j)}), & \tilde{r}_{k,n}^{(j)} = 1. \end{cases} \quad (6)$$

If PF (j, k) did not exist at time $n-1$, i.e., $r_{k,n-1}^{(j)} = 0$, it cannot exist as a legacy PF at time n either. Therefore,

$$f(\tilde{\mathbf{a}}_{k,n}^{(j)}, \tilde{r}_{k,n}^{(j)} | \mathbf{a}_{k,n-1}^{(j)}, r_{k,n-1}^{(j)} = 0) = \begin{cases} f_D(\tilde{\mathbf{a}}_{k,n}^{(j)}), & \tilde{r}_{k,n}^{(j)} = 0 \\ 0, & \tilde{r}_{k,n}^{(j)} = 1. \end{cases} \quad (7)$$

D. Prior Distributions

For a given PA j , there are $M_n^{(j)} = |\mathcal{M}_n^{(j)}|$ new PFs at time n . The number of false alarms is assumed Poisson distributed with mean $\mu_{\text{FA}}^{(j)}$ [23]. Similarly, the number of newly detected features is assumed Poisson distributed with mean $\mu_{\text{n},n}^{(j)}$; the calculation of $\mu_{\text{n},n}^{(j)}$ will be discussed in Section VI. Then, one can derive the following expression of the joint conditional prior probability mass function (pmf) of the DA vector $\mathbf{c}_n^{(j)}$, the vector of existence indicators of new PFs, $\check{\mathbf{r}}_n^{(j)}$, and the number of measurements or equivalently new PFs, $M_n^{(j)}$, given the state of the mobile agent, \mathbf{x}_n , and the vector of augmented states of legacy PFs, $\tilde{\mathbf{y}}_n^{(j)}$ (cf. [31])

$$p(\mathbf{c}_n^{(j)}, \check{\mathbf{r}}_n^{(j)}, M_n^{(j)} | \mathbf{x}_n, \tilde{\mathbf{y}}_n^{(j)}) = \chi_{\mathbf{c}_n^{(j)}, \check{\mathbf{r}}_n^{(j)}, M_n^{(j)}} \psi(\mathbf{c}_n^{(j)}) \left(\prod_{m \in \mathcal{N}_{\check{\mathbf{r}}_n^{(j)}}} \Gamma_{\mathbf{c}_n^{(j)}}(\check{r}_{m,n}^{(j)}) \right) \left(\prod_{k \in \mathcal{D}_{\mathbf{c}_n^{(j)}, \check{\mathbf{r}}_n^{(j)}}} P_{\text{d}}^{(j)}(\mathbf{x}_n, \mathbf{a}_{k,n}^{(j)}) \right)$$

$$\times \prod_{\substack{k' \in \bar{\mathcal{D}}_{\mathbf{c}_n^{(j)}, \tilde{\mathbf{r}}_n^{(j)}}}} [1(c_{k',n}^{(j)}) - \tilde{r}_{k',n}^{(j)} P_{\text{d}}^{(j)}(\mathbf{x}_n, \tilde{\mathbf{a}}_{k',n}^{(j)})], \quad (8)$$

with $\chi_{\mathbf{c}_n^{(j)}, \tilde{\mathbf{r}}_n^{(j)}, M_n^{(j)}} \triangleq e^{-(\mu_{\text{FA}}^{(j)} + \mu_{n,n}^{(j)})} (\mu_{n,n}^{(j)})^{\left| \mathcal{N}_{\tilde{\mathbf{r}}_n^{(j)}} \right|} (\mu_{\text{FA}}^{(j)})^{M_n^{(j)} - \left| \mathcal{D}_{\mathbf{c}_n^{(j)}, \tilde{\mathbf{r}}_n^{(j)}} \right| - \left| \mathcal{N}_{\tilde{\mathbf{r}}_n^{(j)}} \right|} / M_n^{(j)}!$. Here, $\mathcal{N}_{\tilde{\mathbf{r}}_n^{(j)}}$ denotes the set of existing new PFs, i.e., $\mathcal{N}_{\tilde{\mathbf{r}}_n^{(j)}} \triangleq \{m \in \mathcal{M}_n^{(j)} : \tilde{r}_{m,n}^{(j)} = 1\}$; $\mathcal{D}_{\mathbf{c}_n^{(j)}, \tilde{\mathbf{r}}_n^{(j)}}$ denotes the set of existing legacy PFs for PA j , i.e., $\mathcal{D}_{\mathbf{c}_n^{(j)}, \tilde{\mathbf{r}}_n^{(j)}} \triangleq \{k \in \mathcal{K}_{n-1}^{(j)} : \tilde{r}_{k,n}^{(j)} = 1, c_{k,n}^{(j)} \neq 0\}$; and $\bar{\mathcal{D}}_{\mathbf{c}_n^{(j)}, \tilde{\mathbf{r}}_n^{(j)}} \triangleq \mathcal{K}_{n-1}^{(j)} \setminus \mathcal{D}_{\mathbf{c}_n^{(j)}, \tilde{\mathbf{r}}_n^{(j)}}$. In addition, we define

$$\psi(\mathbf{c}_n^{(j)}) \triangleq \begin{cases} 0, & \exists k, k' \in \mathcal{K}_{n-1}^{(j)} \text{ with } k \neq k' \text{ such that } c_{k,n}^{(j)} = c_{k',n}^{(j)} \neq 0 \\ 1, & \text{otherwise,} \end{cases} \quad (9)$$

$$\Gamma_{\mathbf{c}_n^{(j)}}(\tilde{r}_{m,n}^{(j)}) \triangleq \begin{cases} 0, & \tilde{r}_{m,n}^{(j)} = 1 \text{ and } \exists k \in \mathcal{K}_{n-1}^{(j)} \text{ such that } c_{k,n}^{(j)} = m \\ 1, & \text{otherwise.} \end{cases} \quad (10)$$

Finally, $1(c)$ denotes the indicator function of the event $c = 0$ (i.e., $1(c) = 1$ if $c = 0$ and 0 otherwise). The functions $\psi(\mathbf{c}_n^{(j)})$ and $\Gamma_{\mathbf{c}_n^{(j)}}(\tilde{r}_{m,n}^{(j)})$ enforce our DA assumption from Section III-B, i.e., $\psi(\mathbf{c}_n^{(j)})$ enforces $p(\mathbf{c}_n^{(j)}, \tilde{\mathbf{r}}_n^{(j)}, M_n^{(j)} | \mathbf{x}_n, \tilde{\mathbf{y}}_n^{(j)}) = 0$ if any measurement is associated with more than one legacy PF, and $\Gamma_{\mathbf{c}_n^{(j)}}(\tilde{r}_{m,n}^{(j)})$ enforces $p(\mathbf{c}_n^{(j)}, \tilde{\mathbf{r}}_n^{(j)}, M_n^{(j)} | \mathbf{x}_n, \tilde{\mathbf{y}}_n^{(j)}) = 0$ if a new PF is associated with a measurement m that is also associated with a legacy PF. Because there are no legacy PFs at $n = 1$, $\tilde{\mathbf{y}}_1^{(j)}$ is an empty vector. Therefore, $p(\mathbf{c}_1^{(j)}, \tilde{\mathbf{r}}_1^{(j)}, M_1^{(j)} | \mathbf{x}_1, \tilde{\mathbf{y}}_1^{(j)}) = p(\mathbf{c}_1^{(j)}, \tilde{\mathbf{r}}_1^{(j)}, M_1^{(j)} | \mathbf{x}_1)$. An expression of this pmf can be obtained by replacing in (8) (for $n = 1$) all factors involving $\tilde{\mathbf{y}}_1^{(j)}$ (or, equivalently, $\tilde{\mathbf{a}}_1^{(j)}$ and $\tilde{r}_1^{(j)}$) by 1.

The states of newly detected features are assumed to be a priori independent and identically distributed (iid) according to some pdf $f_{n,n}(\mathbf{a}_{\cdot,n}^{(j)} | \mathbf{x}_n)$, whose calculation will be discussed in Section VI. (Here, $\mathbf{a}_{\cdot,n}^{(j)} \in \mathbb{R}^2$ denotes a generic single-feature position.) The prior pdf of the states of new PFs for PA j , $\tilde{\mathbf{a}}_n^{(j)}$, conditioned on \mathbf{x}_n , $\tilde{\mathbf{r}}_n^{(j)}$, and $M_n^{(j)}$ is then obtained as

$$f(\tilde{\mathbf{a}}_n^{(j)} | \mathbf{x}_n, \tilde{\mathbf{r}}_n^{(j)}, M_n^{(j)}) = \left(\prod_{m \in \bar{\mathcal{N}}_{\tilde{\mathbf{r}}_n^{(j)}}} f_{n,n}(\tilde{\mathbf{a}}_{m,n}^{(j)} | \mathbf{x}_n) \right) \prod_{m' \in \bar{\mathcal{N}}_{\tilde{\mathbf{r}}_n^{(j)}}} f_{\text{D}}(\tilde{\mathbf{a}}_{m,n}^{(j)}), \quad (11)$$

where $\bar{\mathcal{N}}_{\tilde{\mathbf{r}}_n^{(j)}} \triangleq \mathcal{M}_n^{(j)} \setminus \mathcal{N}_{\tilde{\mathbf{r}}_n^{(j)}}$. Note that before the measurements are obtained, $M_n^{(j)}$ and, thus, the length of the vectors $\tilde{\mathbf{a}}_n^{(j)}$ and $\tilde{\mathbf{r}}_n^{(j)}$ (which is $M_n^{(j)}$) is random.

We assume that for the agent state at time $n = 1$, \mathbf{x}_1 , an informative prior pdf $f(\mathbf{x}_1)$ is available. We also assume that the new PF state vector $\tilde{\mathbf{a}}_n^{(j)}$ and the DA vectors $\mathbf{c}_n^{(j)}$ are conditionally independent given the legacy PF state vector $\tilde{\mathbf{a}}_n^{(j)}$. Let us next consider $\mathbf{x}_{n'}$, $\mathbf{y}_{n'}$, $\mathbf{c}_{n'}$, and the numbers-of-measurements vector $\mathbf{m}_{n'} \triangleq [M_{n'}^{(1)} \cdots M_{n'}^{(J)}]^T$ for all time steps $n' = 1, \dots, n$, and

accordingly define the vector $\mathbf{x}_{1:n} \triangleq [\mathbf{x}_1^T \cdots \mathbf{x}_n^T]^T$ and similarly $\mathbf{y}_{1:n}$, $\mathbf{c}_{1:n}$, and $\mathbf{m}_{1:n}$. We then obtain the joint prior pdf as

$$\begin{aligned} f(\mathbf{x}_{1:n}, \mathbf{y}_{1:n}, \mathbf{c}_{1:n}, \mathbf{m}_{1:n}) &= f(\mathbf{x}_1) \left(\prod_{j'=1}^J p(\mathbf{c}_1^{(j')}, \check{\mathbf{r}}_1^{(j')}, M_1^{(j')} | \mathbf{x}_1, \tilde{\mathbf{y}}_1^{(j')}) \right) \prod_{n'=2}^n f(\mathbf{x}_{n'} | \mathbf{x}_{n'-1}) \\ &\quad \times \prod_{j=1}^J f(\tilde{\mathbf{y}}_n^{(j)} | \mathbf{y}_{n'-1}^{(j)}) f(\check{\mathbf{a}}_n^{(j)} | \mathbf{x}_{n'}, \check{\mathbf{r}}_n^{(j)}, M_n^{(j)}) p(\mathbf{c}_n^{(j)}, \check{\mathbf{r}}_n^{(j)}, M_n^{(j)} | \mathbf{x}_{n'}, \tilde{\mathbf{y}}_n^{(j)}), \end{aligned} \quad (12)$$

where the last three factors are given by (6) and (7); (11); and (8), respectively.

E. Likelihood Function

The statistical dependency of the measurements $\mathbf{z}_{m,n}^{(j)}$, i.e., the MPC parameter estimates discussed in Section II, on the states \mathbf{x}_n and $\mathbf{a}_{k,n}^{(j)}$ is characterized by the conditional pdf $f(\mathbf{z}_{m,n}^{(j)} | \mathbf{x}_n, \mathbf{a}_{k,n}^{(j)})$. This conditional pdf depends on the concrete measurement model; an example will be considered in Section VII. The pdf $f(\mathbf{z}_{m,n}^{(j)} | \mathbf{x}_n, \mathbf{a}_{k,n}^{(j)})$ is a central element in the conditional pdf of the total measurement vector $\mathbf{z}_n \triangleq [\mathbf{z}_n^{(1)T} \cdots \mathbf{z}_n^{(J)T}]^T$ given \mathbf{x}_n , $\tilde{\mathbf{y}}_n$, $\check{\mathbf{y}}_n$, \mathbf{c}_n , and \mathbf{m}_n . Assuming that the $\mathbf{z}_n^{(j)}$ are conditionally independent across j given \mathbf{x}_n , $\tilde{\mathbf{y}}_n$, $\check{\mathbf{y}}_n$, \mathbf{c}_n , and \mathbf{m}_n [23], we obtain

$$f(\mathbf{z}_n | \mathbf{x}_n, \tilde{\mathbf{y}}_n, \check{\mathbf{y}}_n, \mathbf{c}_n, \mathbf{m}_n) = \prod_{j=1}^J f(\mathbf{z}_n^{(j)} | \mathbf{x}_n, \tilde{\mathbf{y}}_n^{(j)}, \check{\mathbf{y}}_n^{(j)}, \mathbf{c}_n^{(j)}, M_n^{(j)}), \quad (13)$$

where [23]

$$\begin{aligned} f(\mathbf{z}_n^{(j)} | \mathbf{x}_n, \tilde{\mathbf{y}}_n^{(j)}, \check{\mathbf{y}}_n^{(j)}, \mathbf{c}_n^{(j)}, M_n^{(j)}) &= \left(\prod_{m=1}^{M_n^{(j)}} f_{\text{FA}}(\mathbf{z}_{m,n}^{(j)}) \right) \left(\prod_{k \in \mathcal{D}_{\mathbf{c}_n^{(j)}, \check{\mathbf{r}}_n^{(j)}}} \frac{f(\mathbf{z}_{c_{k,n}^{(j)}, n}^{(j)} | \mathbf{x}_n, \check{\mathbf{a}}_{k,n}^{(j)})}{f_{\text{FA}}(\mathbf{z}_{c_{k,n}^{(j)}, n}^{(j)})} \right) \\ &\quad \times \prod_{m' \in \mathcal{N}_{\check{\mathbf{r}}_n^{(j)}}} \frac{f(\mathbf{z}_{m',n}^{(j)} | \mathbf{x}_n, \check{\mathbf{a}}_{m',n}^{(j)})}{f_{\text{FA}}(\mathbf{z}_{m',n}^{(j)})}. \end{aligned} \quad (14)$$

In particular, at $n = 1$, $f(\mathbf{z}_1^{(j)} | \mathbf{x}_1, \tilde{\mathbf{y}}_1^{(j)}, \check{\mathbf{y}}_1^{(j)}, \mathbf{c}_1^{(j)}, M_1^{(j)}) = f(\mathbf{z}_1^{(j)} | \mathbf{x}_1, \check{\mathbf{y}}_1^{(j)}, \mathbf{c}_1^{(j)}, M_1^{(j)})$. An expression of this pdf can be obtained by replacing in (14) (for $n = 1$) all factors involving $\tilde{\mathbf{y}}_1^{(j)}$ (or, equivalently, $\check{\mathbf{a}}_1^{(j)}$ and $\check{\mathbf{r}}_1^{(j)}$) by 1.

Let us consider $f(\mathbf{z}_n^{(j)} | \mathbf{x}_n, \tilde{\mathbf{y}}_n^{(j)}, \check{\mathbf{y}}_n^{(j)}, \mathbf{c}_n^{(j)}, M_n^{(j)})$ as a *likelihood function*, i.e., a function of \mathbf{x}_n , $\tilde{\mathbf{y}}_n^{(j)}$, $\check{\mathbf{y}}_n^{(j)}$, $\mathbf{c}_n^{(j)}$, and $M_n^{(j)}$, for observed $\mathbf{z}_n^{(j)}$. If $\mathbf{z}_n^{(j)}$ is observed and therefore fixed, also $M_n^{(j)}$ is fixed, and we can rewrite (14), up to a constant normalization factor, as

$$f(\mathbf{z}_n^{(j)} | \mathbf{x}_n, \tilde{\mathbf{y}}_n^{(j)}, \check{\mathbf{y}}_n^{(j)}, \mathbf{c}_n^{(j)}, M_n^{(j)}) \propto \left(\prod_{k=1}^{K_n^{(j)}} g_1(\mathbf{x}_n, \tilde{\mathbf{a}}_{k,n}^{(j)}, \tilde{r}_{k,n}^{(j)}, c_{k,n}^{(j)}; \mathbf{z}_n^{(j)}) \right) \prod_{m \in \mathcal{N}_{\tilde{\mathbf{r}}_n^{(j)}}} \frac{f(\mathbf{z}_{m,n}^{(j)} | \mathbf{x}_n, \check{\mathbf{a}}_{m,n}^{(j)})}{f_{\text{FA}}(\mathbf{z}_{m,n}^{(j)})}. \quad (15)$$

Here, the factors $g_1(\mathbf{x}_n, \tilde{\mathbf{a}}_{k,n}^{(j)}, \tilde{r}_{k,n}^{(j)}, c_{k,n}^{(j)}; \mathbf{z}_n^{(j)})$ are defined as

$$g_1(\mathbf{x}_n, \tilde{\mathbf{a}}_{k,n}^{(j)}, 1, c_{k,n}^{(j)}; \mathbf{z}_n^{(j)}) \triangleq \begin{cases} \frac{f(\mathbf{z}_{m,n}^{(j)} | \mathbf{x}_n, \tilde{\mathbf{a}}_{k,n}^{(j)})}{f_{\text{FA}}(\mathbf{z}_{m,n}^{(j)})}, & c_{k,n}^{(j)} \in \mathcal{M}_n^{(j)} \\ 1, & c_{k,n}^{(j)} = 0 \end{cases} \quad (16)$$

$$g_1(\mathbf{x}_n, \tilde{\mathbf{a}}_{k,n}^{(j)}, 0, c_{k,n}^{(j)}; \mathbf{z}_n^{(j)}) \triangleq 1.$$

Finally, the joint likelihood function for $\mathbf{z}_{1:n} \triangleq [\mathbf{z}_1^T \cdots \mathbf{z}_n^T]^T$, involving the measurements $\mathbf{z}_{m,n'}$ of all PAs $j = 1, \dots, J$ and all time steps $n' = 1, \dots, n$, can be derived similarly to (12); one obtains

$$\begin{aligned} f(\mathbf{z}_{1:n} | \mathbf{x}_{1:n}, \mathbf{y}_{1:n}, \mathbf{c}_{1:n}, \mathbf{m}_{1:n}) &\propto \prod_{j=1}^J \left(\prod_{m \in \mathcal{N}_{\tilde{\mathbf{r}}_1^{(j)}}} \frac{f(\mathbf{z}_{m,1}^{(j)} | \mathbf{x}_1, \check{\mathbf{a}}_{m,1}^{(j)})}{f_{\text{FA}}(\mathbf{z}_{m,1}^{(j)})} \right) \prod_{n'=2}^n \left(\prod_{m' \in \mathcal{N}_{\tilde{\mathbf{r}}_n^{(j)}}} \frac{f(\mathbf{z}_{m',n'}^{(j)} | \mathbf{x}_{n'}, \check{\mathbf{a}}_{m',n'}^{(j)})}{f_{\text{FA}}(\mathbf{z}_{m',n'}^{(j)})} \right) \\ &\times \prod_{k=1}^{K_{n'}^{(j)}} g_1(\mathbf{x}_{n'}, \tilde{\mathbf{a}}_{k,n'}^{(j)}, \tilde{r}_{k,n'}^{(j)}, c_{k,n'}^{(j)}; \mathbf{z}_{n'}^{(j)}). \end{aligned} \quad (17)$$

IV. JOINT POSTERIOR PDF AND FACTOR GRAPH

A. Redundant Formulation of the Exclusion Constraint

The proposed BP algorithm is based on a redundant formulation of probabilistic DA that involves both the feature-oriented DA vectors $\mathbf{c}_n^{(j)}$ and the measurement-oriented DA vectors $\mathbf{b}_n^{(j)}$ [30], [31]. To obtain a corresponding probabilistic description and, in turn, a factor graph, we formally replace the exclusion constraint factor $\psi(\mathbf{c}_n^{(j)})$ involved in the prior pmf in (8) by

$$\psi(\mathbf{c}_n^{(j)}, \mathbf{b}_n^{(j)}) \triangleq \prod_{k=1}^{K_n^{(j)}} \prod_{m=1}^{M_n^{(j)}} \psi(c_{k,n}^{(j)}, b_{m,n}^{(j)}), \quad (18)$$

with the indicator function

$$\psi(c_{k,n}^{(j)}, b_{m,n}^{(j)}) \triangleq \begin{cases} 0, & c_{k,n}^{(j)} = m, b_{m,n}^{(j)} \neq k \text{ or } b_{m,n}^{(j)} = k, c_{k,n}^{(j)} \neq m \\ 1, & \text{else.} \end{cases} \quad (19)$$

The resulting modified prior pmf $p(\mathbf{c}_n^{(j)}, \mathbf{b}_n^{(j)}, \check{\mathbf{r}}_n^{(j)}, M_n^{(j)} | \mathbf{x}_n, \tilde{\mathbf{y}}_n^{(j)})$ is related to the original prior pmf $p(\mathbf{c}_n^{(j)}, \check{\mathbf{r}}_n^{(j)}, M_n^{(j)} | \mathbf{x}_n, \tilde{\mathbf{y}}_n^{(j)})$ in (8) according to $p(\mathbf{c}_n^{(j)}, \check{\mathbf{r}}_n^{(j)}, M_n^{(j)} | \mathbf{x}_n, \tilde{\mathbf{y}}_n^{(j)}) = \sum_{\mathbf{b}_n^{(j)}} p(\mathbf{c}_n^{(j)}, \mathbf{b}_n^{(j)}, \check{\mathbf{r}}_n^{(j)}, M_n^{(j)} | \mathbf{x}_n, \tilde{\mathbf{y}}_n^{(j)})$, where the summation is over all $\mathbf{b}_n^{(j)} \in \{0, 1, \dots, K_n^{(j)}\}^{M_n^{(j)}}$.

Let us now consider the product of the likelihood function $f(\mathbf{z}_n^{(j)} | \mathbf{x}_n, \tilde{\mathbf{y}}_n^{(j)}, \check{\mathbf{y}}_n^{(j)}, \mathbf{c}_n^{(j)}, M_n^{(j)})$ in (15), the prior pdf of the new PF states $f(\check{\mathbf{a}}_n^{(j)} | \mathbf{x}_n, \check{\mathbf{r}}_n^{(j)}, M_n^{(j)})$ in (11), and the modified prior pmf $p(\mathbf{c}_n^{(j)}, \mathbf{b}_n^{(j)}, \check{\mathbf{r}}_n^{(j)}, M_n^{(j)} | \mathbf{x}_n, \tilde{\mathbf{y}}_n^{(j)})$. We obtain

$$\begin{aligned} & f(\mathbf{z}_n^{(j)} | \mathbf{x}_n, \tilde{\mathbf{y}}_n^{(j)}, \check{\mathbf{y}}_n^{(j)}, \mathbf{c}_n^{(j)}, M_n^{(j)}) f(\check{\mathbf{a}}_n^{(j)} | \mathbf{x}_n, \check{\mathbf{r}}_n^{(j)}, M_n^{(j)}) p(\mathbf{c}_n^{(j)}, \mathbf{b}_n^{(j)}, \check{\mathbf{r}}_n^{(j)}, M_n^{(j)} | \mathbf{x}_n, \tilde{\mathbf{y}}_n^{(j)}) \\ & \propto \psi(\mathbf{c}_n^{(j)}, \mathbf{b}_n^{(j)}) \left(\prod_{k=1}^{K_n^{(j)}} g(\mathbf{x}_n, \tilde{\mathbf{a}}_{k,n}^{(j)}, \tilde{r}_{k,n}^{(j)}, c_{k,n}^{(j)}; \mathbf{z}_n^{(j)}) \right) \left(\prod_{m' \in \bar{\mathcal{N}}_{\check{\mathbf{r}}_n^{(j)}}} f_{\text{D}}(\check{\mathbf{a}}_{m',n}^{(j)}) \right) \\ & \times \prod_{m \in \mathcal{N}_{\check{\mathbf{r}}_n^{(j)}}} \frac{\mu_{\text{n},n}^{(j)} f_{\text{n},n}(\check{\mathbf{a}}_{m,n}^{(j)} | \mathbf{x}_n) \Gamma_{\mathbf{c}_n^{(j)}}(\check{r}_{m,n}^{(j)}) f(\mathbf{z}_{m,n}^{(j)} | \mathbf{x}_n, \check{\mathbf{a}}_{m,n}^{(j)})}{f_{\text{FA}}(\mathbf{z}_{m,n}^{(j)})}. \end{aligned} \quad (20)$$

Here, $g(\mathbf{x}_n, \tilde{\mathbf{a}}_{k,n}^{(j)}, \tilde{r}_{k,n}^{(j)}, c_{k,n}^{(j)}; \mathbf{z}_n^{(j)}) \triangleq g_1(\mathbf{x}_n, \tilde{\mathbf{a}}_{k,n}^{(j)}, \tilde{r}_{k,n}^{(j)}, c_{k,n}^{(j)}; \mathbf{z}_n^{(j)}) g_2(\mathbf{x}_n, \tilde{\mathbf{a}}_{k,n}^{(j)}, \tilde{r}_{k,n}^{(j)}, c_{k,n}^{(j)}; M_n^{(j)})$, where $g_1(\mathbf{x}_n, \tilde{\mathbf{a}}_{k,n}^{(j)}, \tilde{r}_{k,n}^{(j)}, c_{k,n}^{(j)}; \mathbf{z}_n^{(j)})$ was defined in (16) and $g_2(\mathbf{x}_n, \tilde{\mathbf{a}}_{k,n}^{(j)}, \tilde{r}_{k,n}^{(j)}, c_{k,n}^{(j)}; M_n^{(j)})$ is defined as

$$g_2(\mathbf{x}_n, \tilde{\mathbf{a}}_{k,n}^{(j)}, 1, c_{k,n}^{(j)}; M_n^{(j)}) \triangleq \begin{cases} \frac{P_{\text{d}}^{(j)}(\mathbf{x}_n, \tilde{\mathbf{a}}_{k,n}^{(j)})}{\mu_{\text{FA}}^{(j)}}, & c_{k,n}^{(j)} \in \mathcal{M}_n^{(j)} \\ 1 - P_{\text{d}}^{(j)}(\mathbf{x}_n, \tilde{\mathbf{a}}_{k,n}^{(j)}), & c_{k,n}^{(j)} = 0 \end{cases} \quad (21)$$

$$g_2(\mathbf{x}_n, \tilde{\mathbf{a}}_{k,n}^{(j)}, 0, c_{k,n}^{(j)}; M_n^{(j)}) \triangleq 1(c_{k,n}^{(j)}).$$

One thus obtains for $g(\mathbf{x}_n, \tilde{\mathbf{a}}_{k,n}^{(j)}, \tilde{r}_{k,n}^{(j)}, c_{k,n}^{(j)}; \mathbf{z}_n^{(j)})$

$$g(\mathbf{x}_n, \tilde{\mathbf{a}}_{k,n}^{(j)}, 1, c_{k,n}^{(j)}; \mathbf{z}_n^{(j)}) = \begin{cases} \frac{P_{\text{d}}^{(j)}(\mathbf{x}_n, \tilde{\mathbf{a}}_{k,n}^{(j)}) f(\mathbf{z}_{m,n}^{(j)} | \mathbf{x}_n, \tilde{\mathbf{a}}_{k,n}^{(j)})}{\mu_{\text{FA}}^{(j)} f_{\text{FA}}(\mathbf{z}_{m,n}^{(j)})}, & c_{k,n}^{(j)} \in \mathcal{M}_n^{(j)} \\ 1 - P_{\text{d}}^{(j)}(\mathbf{x}_n, \tilde{\mathbf{a}}_{k,n}^{(j)}), & c_{k,n}^{(j)} = 0 \end{cases} \quad (22)$$

$$g(\mathbf{x}_n, \tilde{\mathbf{a}}_{k,n}^{(j)}, 0, c_{k,n}^{(j)}; \mathbf{z}_n^{(j)}) = 1(c_{k,n}^{(j)}).$$

For a choice of $\mathbf{c}_n^{(j)}$ and $\mathbf{b}_n^{(j)}$ that is valid in the sense that $p(\mathbf{c}_n^{(j)}, \mathbf{b}_n^{(j)}, \check{\mathbf{r}}_n^{(j)}, M_n^{(j)} | \mathbf{x}_n, \tilde{\mathbf{y}}_n^{(j)}) \neq 0$, the exclusion constraint expressed by $\Gamma_{\mathbf{c}_n^{(j)}}(\check{r}_{m,n}^{(j)})$ is satisfied, i.e., $\Gamma_{\mathbf{c}_n^{(j)}}(\check{r}_{m,n}^{(j)}) = 1$, if and only if both $b_{m,n}^{(j)} = 0$ and $\check{r}_{m,n}^{(j)} = 1$. Therefore, in (20), we can summarize the products over all $m \in \mathcal{N}_{\check{\mathbf{r}}_n^{(j)}}$ and over all $m' \in \bar{\mathcal{N}}_{\check{\mathbf{r}}_n^{(j)}}$ by a product over all $m \in \mathcal{M}_n^{(j)} = \{1, \dots, M_n^{(j)}\}$. More specifically, we can rewrite (20) as

$$f(\mathbf{z}_n^{(j)} | \mathbf{x}_n, \tilde{\mathbf{y}}_n^{(j)}, \check{\mathbf{y}}_n^{(j)}, \mathbf{c}_n^{(j)}, M_n^{(j)}) f(\check{\mathbf{a}}_n^{(j)} | \mathbf{x}_n, \check{\mathbf{r}}_n^{(j)}, M_n^{(j)}) p(\mathbf{c}_n^{(j)}, \mathbf{b}_n^{(j)}, \check{\mathbf{r}}_n^{(j)}, M_n^{(j)} | \mathbf{x}_n, \tilde{\mathbf{y}}_n^{(j)})$$

$$\propto \psi(\mathbf{c}_n^{(j)}, \mathbf{b}_n^{(j)}) \left(\prod_{k=1}^{K_n^{(j)}} g(\mathbf{x}_n, \tilde{\mathbf{a}}_{k,n}^{(j)}, \tilde{r}_{k,n}^{(j)}, c_{k,n}^{(j)}; \mathbf{z}_n^{(j)}) \right) \prod_{m=1}^{M_n^{(j)}} h(\mathbf{x}_n, \breve{\mathbf{a}}_{m,n}^{(j)}, \breve{r}_{m,n}^{(j)}, b_{m,n}^{(j)}; \mathbf{z}_n^{(j)}), \quad (23)$$

where $h(\mathbf{x}_n, \breve{\mathbf{a}}_{m,n}^{(j)}, \breve{r}_{m,n}^{(j)}, b_{m,n}^{(j)}; \mathbf{z}_n^{(j)})$ is defined as

$$h(\mathbf{x}_n, \breve{\mathbf{a}}_{m,n}^{(j)}, 1, b_{m,n}^{(j)}; \mathbf{z}_n^{(j)}) \triangleq \begin{cases} 0, & b_{m,n}^{(j)} \in \mathcal{K}_n^{(j)} \\ \frac{\mu_{n,n}^{(j)} f_{n,n}(\breve{\mathbf{a}}_{m,n}^{(j)} | \mathbf{x}_n) f(\mathbf{z}_{m,n}^{(j)} | \mathbf{x}_n, \breve{\mathbf{a}}_{m,n}^{(j)})}{\mu_{\text{FA}}^{(j)} f_{\text{FA}}(\mathbf{z}_{m,n}^{(j)})}, & b_{m,n}^{(j)} = 0 \end{cases} \quad (24)$$

$$h(\mathbf{x}_n, \breve{\mathbf{a}}_{m,n}^{(j)}, 0, b_{m,n}^{(j)}; \mathbf{z}_n^{(j)}) \triangleq f_{\text{D}}(\breve{\mathbf{a}}_{m,n}^{(j)}).$$

The calculation of $\mu_{n,n}^{(j)} f_{n,n}(\breve{\mathbf{a}}_{m,n}^{(j)} | \mathbf{x}_n)$ will be discussed in Section VI.

B. Joint Posterior pdf

Using Bayes' rule and common independence assumptions [23], [39], the joint posterior pdf of $\mathbf{x}_{n'}, \tilde{\mathbf{y}}_{n'}, \breve{\mathbf{y}}_{n'}, \mathbf{c}_{n'},$ and $\mathbf{b}_{n'}$ for all time steps $n' = 1, \dots, n$ is obtained as

$$\begin{aligned} & f(\mathbf{x}_{1:n}, \mathbf{y}_{1:n}, \mathbf{c}_{1:n}, \mathbf{b}_{1:n}, \mathbf{m}_{1:n} | \mathbf{z}_{1:n}) \\ & \propto f(\mathbf{z}_{1:n} | \mathbf{x}_{1:n}, \mathbf{y}_{1:n}, \mathbf{c}_{1:n}, \mathbf{m}_{1:n}) f(\mathbf{x}_{1:n}, \mathbf{y}_{1:n}, \mathbf{c}_{1:n}, \mathbf{m}_{1:n}) \\ & = f(\mathbf{x}_1) \left(\prod_{j'=1}^J f(\mathbf{z}_1^{(j')} | \mathbf{x}_1, \breve{\mathbf{y}}_1^{(j')}, \mathbf{c}_1^{(j')}, M_1^{(j')}) f(\breve{\mathbf{y}}_1^{(j')}, \mathbf{c}_1^{(j')}, M_1^{(j')}) \right) \\ & \times \prod_{n'=2}^n f(\mathbf{x}_{n'} | \mathbf{x}_{n'-1}) \prod_{j=1}^J f(\tilde{\mathbf{y}}_{n'}^{(j)} | \mathbf{y}_{n'-1}^{(j)}) f(\mathbf{z}_{n'}^{(j)} | \mathbf{x}_{n'}, \tilde{\mathbf{y}}_{n'}^{(j)}, \breve{\mathbf{y}}_{n'}^{(j)}, \mathbf{c}_{n'}^{(j)}, M_{n'}^{(j)}) \\ & \times f(\breve{\mathbf{a}}_{n'}^{(j)} | \mathbf{x}_{n'}, \breve{r}_{n'}^{(j)}, M_{n'}^{(j)}) p(\mathbf{c}_{n'}^{(j)}, \mathbf{b}_{n'}^{(j)}, \breve{r}_{n'}^{(j)}, M_{n'}^{(j)} | \mathbf{x}_{n'}, \tilde{\mathbf{y}}_{n'}^{(j)}). \end{aligned} \quad (25)$$

Inserting expression (23) yields

$$\begin{aligned} & f(\mathbf{x}_{1:n}, \mathbf{y}_{1:n}, \mathbf{c}_{1:n}, \mathbf{b}_{1:n}, \mathbf{m}_{1:n} | \mathbf{z}_{1:n}) \\ & \propto f(\mathbf{x}_1) \left(\prod_{j'=1}^J \prod_{m'=1}^{M_1^{(j')}} h(\mathbf{x}_1, \breve{\mathbf{a}}_{m',1}^{(j')}, \breve{r}_{m',1}^{(j')}, b_{m',1}^{(j')}; \mathbf{z}_1^{(j')}) \right) \\ & \times \prod_{n'=2}^n f(\mathbf{x}_{n'} | \mathbf{x}_{n'-1}) \prod_{j=1}^J \psi(\mathbf{c}_{n'}^{(j)}, \mathbf{b}_{n'}^{(j)}) f(\breve{\mathbf{y}}_{n'}^{(j)} | \mathbf{y}_{n'-1}^{(j)}) \left(\prod_{m=1}^{M_{n'}^{(j)}} h(\mathbf{x}_{n'}, \breve{\mathbf{a}}_{m,n'}^{(j)}, \breve{r}_{m,n'}^{(j)}, b_{m,n'}^{(j)}; \mathbf{z}_{n'}^{(j)}) \right) \\ & \times \prod_{k=1}^{K_{n'}^{(j)}} g(\mathbf{x}_{n'}, \tilde{\mathbf{a}}_{k,n'}^{(j)}, \tilde{r}_{k,n'}^{(j)}, c_{k,n'}^{(j)}; \mathbf{z}_{n'}^{(j)}). \end{aligned} \quad (26)$$

This factorization of the joint posterior pdf is represented by the factor graph [28], [29] shown in Fig. 2.

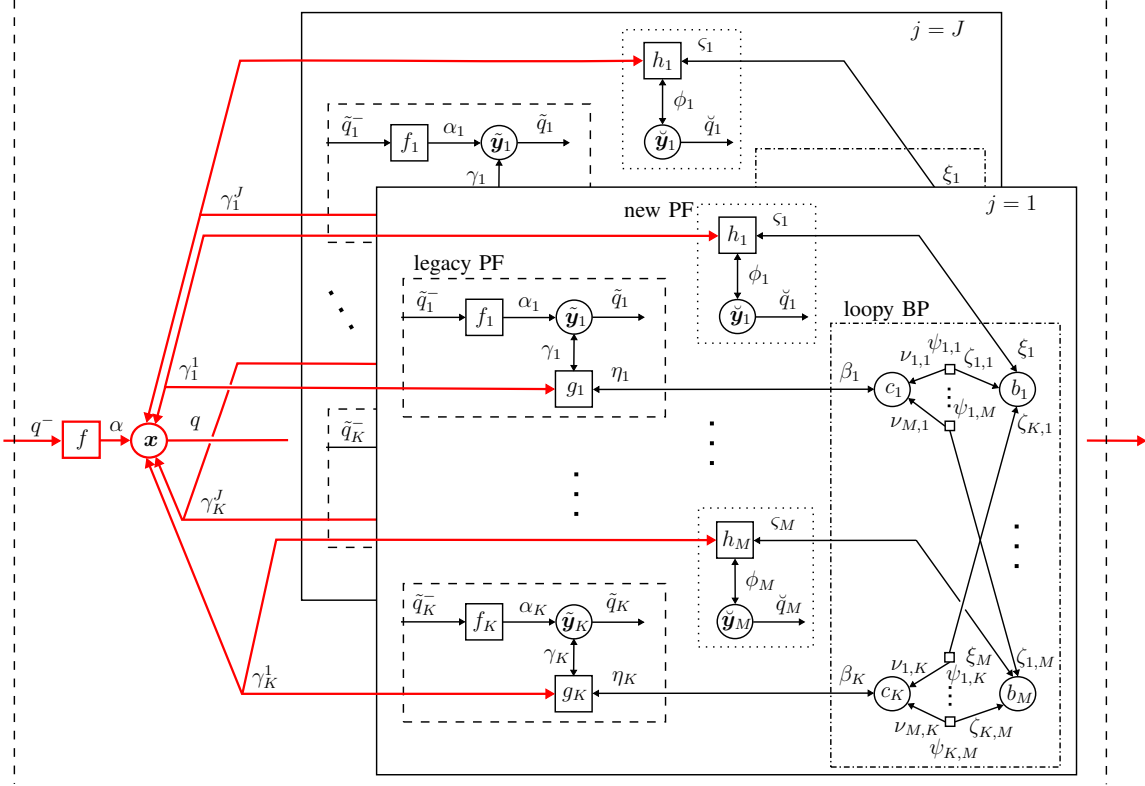


Fig. 2: Factor graph representing the factorization of the joint posterior pdf in (26). The red boldface part represents all factor nodes and variable nodes related to the agent state, and the black part all factor nodes, variable nodes, and messages related to the PF states. The dashed boxes contain the parts of the factor graph related to legacy PFs, the dotted boxes the parts related to new PFs, and the dashed-dotted boxes the parts related to DA. The following short notations are used: $K \triangleq K_n^{(j)}$, $M \triangleq M_n^{(j)}$, $\mathbf{x} \triangleq \mathbf{x}_n$, $\tilde{\mathbf{y}}_k \triangleq \tilde{\mathbf{y}}_{k,n}^{(j)}$, $\tilde{\mathbf{y}}_m \triangleq \tilde{\mathbf{y}}_{m,n}^{(j)}$, $b_m \triangleq b_{m,n}^{(j)}$, $c_k \triangleq c_{k,n}^{(j)}$, $\psi_{k,m} \triangleq \psi(c_{k,n}^{(j)}, b_{m,n}^{(j)})$, $g_k \triangleq g(\mathbf{x}_n, \tilde{\mathbf{a}}_{k,n}^{(j)}, \tilde{r}_{k,n}^{(j)}, c_{k,n}^{(j)}; \mathbf{z}_n^{(j)})$, $h_m \triangleq h(\mathbf{x}_n, \tilde{\mathbf{a}}_{m,n}^{(j)}, \tilde{r}_{m,n}^{(j)}, b_{m,n}^{(j)}; \mathbf{z}_n^{(j)})$, $f \triangleq f(\mathbf{x}_n | \mathbf{x}_{n-1})$, $f_k \triangleq f(\mathbf{y}_{k,n}^{(j)} | \mathbf{y}_{k,n-1}^{(j)})$, $\alpha \triangleq \alpha(\mathbf{x}_n)$, $\alpha_k \triangleq \alpha_k(\tilde{\mathbf{a}}_{k,n}^{(j)}, \tilde{r}_{k,n}^{(j)})$, $q^- \triangleq q(\mathbf{x}_{n-1})$, $q \triangleq q(\mathbf{x}_n)$, $\tilde{q}_k^- \triangleq \tilde{q}(\tilde{\mathbf{a}}_{k,n-1}^{(j)}, \tilde{r}_{k,n-1}^{(j)})$, $\tilde{q}_k \triangleq \tilde{q}(\tilde{\mathbf{a}}_{k,n}^{(j)}, \tilde{r}_{k,n}^{(j)})$, $\tilde{q}_m \triangleq \tilde{q}(\tilde{\mathbf{a}}_{m,n}^{(j)}, \tilde{r}_{m,n}^{(j)})$, $\beta_k \triangleq \beta(c_{k,n}^{(j)})$, $\xi_m \triangleq \xi(b_{m,n}^{(j)})$, $\eta_k \triangleq \eta(c_{k,n}^{(j)})$, $\varsigma_m \triangleq \varsigma(b_{m,n}^{(j)})$, $\nu_{m,k} \triangleq \nu_{m \rightarrow k}(c_{k,n}^{(j)})$, $\zeta_{k,m} \triangleq \zeta_{k \rightarrow m}(b_{m,n}^{(j)})$, $\gamma_k^j \triangleq \gamma_k^{(j)}(\mathbf{x}_n)$, $\gamma_k \triangleq \gamma(\tilde{\mathbf{a}}_{k,n}^{(j)}, \tilde{r}_{k,n}^{(j)})$, and $\phi_m \triangleq \phi(\tilde{\mathbf{a}}_{m,n}^{(j)}, \tilde{r}_{m,n}^{(j)})$.

V. BP ALGORITHM FOR SLAM

In this section, we first discuss the procedure used for PF detection and state estimation. Subsequently, we develop a BP message passing algorithm for approximate calculation of the marginal posterior distributions required for detection and estimation.

A. Detection and Estimation

Our goal is to estimate the agent state \mathbf{x}_n and to detect and estimate the PF states $\mathbf{a}_{k,n}^{(j)}$ from all the past and present measurements, i.e., from the total measurement vector $\mathbf{z}_{1:n}$. In the Bayesian framework, estimation of the agent state \mathbf{x}_n at time n is based on the posterior pdf $f(\mathbf{x}_n | \mathbf{z}_{1:n})$.

More specifically, we will develop an approximate calculation of the minimum mean-square error (MMSE) estimator [40]

$$\hat{\mathbf{x}}_n^{\text{MMSE}} \triangleq \int \mathbf{x}_n f(\mathbf{x}_n | \mathbf{z}_{1:n}) d\mathbf{x}_n. \quad (27)$$

Furthermore, detecting (i.e., determining the existence of) PF $k \in \mathcal{K}_n^{(j)}$ at time n is based on the posterior existence probability $p(r_{k,n}^{(j)} = 1 | \mathbf{z}_{1:n})$. This probability can be obtained from the posterior pdf of the augmented PF state, $f(\mathbf{y}_{k,n}^{(j)} | \mathbf{z}_{1:n}) = f(\mathbf{a}_{k,n}^{(j)}, r_{k,n}^{(j)} | \mathbf{z}_{1:n})$, by a marginalization

$$p(r_{k,n}^{(j)} = 1 | \mathbf{z}_{1:n}) = \int f(\mathbf{a}_{k,n}^{(j)}, r_{k,n}^{(j)} = 1 | \mathbf{z}_{1:n}) d\mathbf{a}_{k,n}^{(j)}. \quad (28)$$

Then PF k is defined to be detected at time n if $p(r_{k,n}^{(j)} = 1 | \mathbf{z}_{1:n}) > P_{\text{det}}$, where P_{det} is a detection threshold. The states $\mathbf{a}_{k,n}^{(j)}$ of the detected PFs are estimated as

$$\hat{\mathbf{a}}_{k,n}^{(j)\text{MMSE}} \triangleq \int \mathbf{a}_{k,n}^{(j)} f(\mathbf{a}_{k,n}^{(j)} | r_{k,n}^{(j)} = 1, \mathbf{z}_{1:n}) d\mathbf{a}_{k,n}^{(j)}, \quad (29)$$

where

$$f(\mathbf{a}_{k,n}^{(j)} | r_{k,n}^{(j)} = 1, \mathbf{z}_{1:n}) = \frac{f(\mathbf{a}_{k,n}^{(j)}, r_{k,n}^{(j)} = 1 | \mathbf{z}_{1:n})}{p(r_{k,n}^{(j)} = 1 | \mathbf{z}_{1:n})}. \quad (30)$$

The posterior existence probabilities $p(r_{k,n}^{(j)} = 1 | \mathbf{z}_{1:n})$ in (28) are also used in a different context. To prevent an indefinite increase of the total number of PFs for PA j due to (2), i.e., $K_n^{(j)} = K_{n-1}^{(j)} + M_n^{(j)}$, a pruning of the PFs is employed. More specifically, PF k is retained only if $p(r_{k,n}^{(j)} = 1 | \mathbf{z}_{1:n})$ exceeds a suitably chosen pruning threshold P_{prun} .

B. BP Message Passing Algorithm

The expressions (27), (28), and (29) involve the posterior pdfs $f(\mathbf{x}_n | \mathbf{z}_{1:n})$ and $f(\mathbf{a}_{k,n}^{(j)}, r_{k,n}^{(j)} | \mathbf{z}_{1:n})$, which are marginal pdfs of the joint posterior pdf $f(\mathbf{x}_{1:n}, \mathbf{y}_{1:n}, \mathbf{c}_{1:n}, \mathbf{b}_{1:n}, \mathbf{m}_{1:n} | \mathbf{z}_{1:n})$ in (26). However, direct marginalization of the joint posterior pdf is infeasible. Therefore, the marginal pdfs $f(\mathbf{x}_n | \mathbf{z}_{1:n})$ and $f(\mathbf{a}_{k,n}^{(j)}, r_{k,n}^{(j)} | \mathbf{z}_{1:n})$ are approximated by means of an efficient BP message passing algorithm. This algorithm is derived by applying the sum-product algorithm [29] to the factor graph in Fig. 2. Since the factor graph contains loops, the sum-product algorithm is used in an iterative manner, and the resulting beliefs are only approximations of the respective posterior pdfs. Furthermore, there is no canonical order in which the messages should be computed, and different orders may lead to different beliefs. In our method, we choose the order according to the following rules: (i) Messages are not passed backward in time; (ii) *iterative* message passing is only performed for DA, and only for each time step and for each PA separately

(i.e., in particular, for the loops connecting different PAs, we only perform a single message passing iteration); (iii) along an edge connecting an agent state variable node and a new PF state variable node, messages are only sent from the former to the latter. Using the message passing schedule resulting from these rules, the sum-product algorithm leads to the message passing and calculation scheme presented in what follows; see also Fig. 2.

First, a prediction step is performed. The prediction message for the agent state is obtained as

$$\alpha(\mathbf{x}_n) = \int f(\mathbf{x}_n | \mathbf{x}_{n-1}) q(\mathbf{x}_{n-1}) d\mathbf{x}_{n-1}, \quad (31)$$

and the prediction message for the legacy PFs is obtained as

$$\alpha_k(\tilde{\mathbf{a}}_{k,n}^{(j)}, \tilde{r}_{k,n}^{(j)}) = \sum_{r_{k,n-1}^{(j)} \in \{0,1\}} \int f(\tilde{\mathbf{a}}_{k,n}^{(j)}, \tilde{r}_{k,n}^{(j)} | \mathbf{a}_{k,n-1}^{(j)}, r_{k,n-1}^{(j)}) \tilde{q}(\mathbf{a}_{k,n-1}^{(j)}, r_{k,n-1}^{(j)}) d\mathbf{a}_{k,n-1}^{(j)}, \quad (32)$$

where the beliefs $q(\mathbf{x}_{n-1})$ and $\tilde{q}(\mathbf{a}_{k,n-1}^{(j)}, 1)$ were calculated at the preceding time $n-1$. Inserting (6) and (7) for $f(\tilde{\mathbf{a}}_{k,n}^{(j)}, \tilde{r}_{k,n}^{(j)} | \mathbf{a}_{k,n-1}^{(j)}, r_{k,n-1}^{(j)} = 1)$ and $f(\tilde{\mathbf{a}}_{k,n}^{(j)}, \tilde{r}_{k,n}^{(j)} | \mathbf{a}_{k,n-1}^{(j)}, r_{k,n-1}^{(j)} = 0)$, respectively, we obtain for $r_{k,n}^{(j)} = 1$

$$\alpha_k(\tilde{\mathbf{a}}_{k,n}^{(j)}, 1) = P_s \int f(\tilde{\mathbf{a}}_{k,n}^{(j)} | \mathbf{a}_{k,n-1}^{(j)}) \tilde{q}(\mathbf{a}_{k,n-1}^{(j)}, 1) d\mathbf{a}_{k,n-1}^{(j)}, \quad (33)$$

and for $r_{k,n}^{(j)} = 0$

$$\alpha_{k,n}^{(j)} = (1 - P_s) \int \tilde{q}(\mathbf{a}_{k,n-1}^{(j)}, 1) d\mathbf{a}_{k,n-1}^{(j)} + \tilde{q}_{k,n-1}^{(j)}, \quad (34)$$

where $\alpha_{k,n}^{(j)} \triangleq \int \alpha_k(\mathbf{a}_{k,n}^{(j)}, 0) d\mathbf{a}_{k,n}^{(j)}$ and $\tilde{q}_{k,n-1}^{(j)} \triangleq \int \tilde{q}(\mathbf{a}_{k,n-1}^{(j)}, 0) d\mathbf{a}_{k,n-1}^{(j)}$.

After the prediction step, the following calculations are performed for all legacy PFs $k \in \mathcal{K}_{n-1}^{(j)}$ and for all new PFs $m \in \mathcal{M}_n^{(j)}$ for all PAs $j \in \{1, \dots, J\}$ in parallel:

- 1) *Measurement evaluation for legacy PFs*: The messages $\beta(c_{k,n}^{(j)})$ passed to the variable nodes corresponding to the feature-oriented DA variables $c_{k,n}^{(j)}$ (cf. Fig. 2) are calculated as

$$\beta(c_{k,n}^{(j)}) = \iint \alpha_k(\tilde{\mathbf{a}}_{k,n}^{(j)}, 1) \alpha(\mathbf{x}_n) g(\mathbf{x}_n, \tilde{\mathbf{a}}_{k,n}^{(j)}, 1, c_{k,n}^{(j)}; \mathbf{z}_n^{(j)}) d\mathbf{x}_n d\tilde{\mathbf{a}}_{k,n}^{(j)} + 1(c_{k,n}^{(j)}) \alpha_{k,n}^{(j)}. \quad (35)$$

- 2) *Measurement evaluation for new PFs*: The messages $\xi(b_{m,n}^{(j)})$ passed to the variable nodes corresponding to the measurement-oriented DA variables $b_{m,n}^{(j)}$ are calculated as

$$\xi(b_{m,n}^{(j)}) = \sum_{\check{r}_{m,n}^{(j)} \in \{0,1\}} \iint h(\mathbf{x}_n, \check{\mathbf{a}}_{m,n}^{(j)}, \check{r}_{m,n}^{(j)}, b_{m,n}^{(j)}; \mathbf{z}_n^{(j)}) \alpha(\mathbf{x}_n) d\mathbf{x}_n d\check{\mathbf{a}}_{m,n}^{(j)}. \quad (36)$$

Inserting (24) for $h(\mathbf{x}_n, \check{\mathbf{a}}_{m,n}^{(j)}, \check{r}_{m,n}^{(j)}, b_{m,n}^{(j)}; \mathbf{z}_n^{(j)})$, this expression is easily seen to simplify to $\xi(b_{m,n}^{(j)}) = 1$ for $b_{m,n}^{(j)} \in \mathcal{K}_{n-1}^{(j)}$, and for $b_{m,n}^{(j)} = 0$ it becomes

$$\xi(b_{m,n}^{(j)}) = 1 + \frac{\mu_{n,n}^{(j)}}{\mu_{\text{FA}}^{(j)} f_{\text{FA}}(\mathbf{z}_{m,n}^{(j)})} \iint \alpha(\mathbf{x}_n) f(\mathbf{z}_{m,n}^{(j)} | \mathbf{x}_n, \check{\mathbf{a}}_{m,n}^{(j)}) f_{n,n}(\check{\mathbf{a}}_n^{(j)} | \mathbf{x}_n) d\mathbf{x}_n d\check{\mathbf{a}}_{m,n}^{(j)}. \quad (37)$$

3) *Iterative data association:* Next, from $\beta(c_{k,n}^{(j)})$ and $\xi(b_{m,n}^{(j)})$, messages $\eta(c_{k,n}^{(j)})$ and $\varsigma(b_{m,n}^{(j)})$ are obtained through a loopy (iterative) BP scheme. First, for each measurement $m \in \mathcal{M}_n^{(j)}$, messages $\nu_{m \rightarrow k}^{(p)}(c_{k,n}^{(j)})$ and $\zeta_{k \rightarrow m}^{(p)}(b_{m,n}^{(j)})$ are calculated iteratively according to [30], [32]

$$\nu_{m \rightarrow k}^{(p)}(c_{k,n}^{(j)}) = \sum_{b_{m,n}^{(j)}=0}^{K_{n-1}^{(j)}} \xi(b_{m,n}^{(j)}) \psi(c_{k,n}^{(j)}, b_{m,n}^{(j)}) \prod_{k' \in \mathcal{K}_{n-1}^{(j)} \setminus \{k\}} \zeta_{k' \rightarrow m}^{(p-1)}(b_{m,n}^{(j)}) \quad (38)$$

$$\zeta_{k \rightarrow m}^{(p)}(b_{m,n}^{(j)}) = \sum_{c_{k,n}^{(j)}=0}^{M_n^{(j)}} \beta(c_{k,n}^{(j)}) \psi(c_{k,n}^{(j)}, b_{m,n}^{(j)}) \prod_{m' \in \mathcal{M}_n^{(j)} \setminus \{m\}} \nu_{m' \rightarrow k}^{(p)}(c_{k,n}^{(j)}), \quad (39)$$

for $k = 1, \dots, K_{n-1}^{(j)}$, $m = 1, \dots, M_n^{(j)}$, and iteration index $p = 1, \dots, P$. The recursion defined by (38) and (39) is initialized (for $p = 0$) by

$$\zeta_{k \rightarrow m}^{(0)}(b_{m,n}^{(j)}) = \sum_{c_{k,n}^{(j)}=0}^{M_n^{(j)}} \beta(c_{k,n}^{(j)}) \psi(c_{k,n}^{(j)}, b_{m,n}^{(j)}).$$

Then, after the last iteration $p = P$, the messages $\eta(c_{k,n}^{(j)})$ and $\varsigma(b_{m,n}^{(j)})$ are calculated as

$$\eta(c_{k,n}^{(j)}) = \prod_{m \in \mathcal{M}_n^{(j)}} \nu_{m \rightarrow k}^{(P)}(c_{k,n}^{(j)}), \quad \varsigma(b_{m,n}^{(j)}) = \prod_{k \in \mathcal{K}_{n-1}^{(j)}} \zeta_{k \rightarrow m}^{(P)}(b_{m,n}^{(j)}). \quad (40)$$

4) *Measurement update for the agent:* From $\eta(c_{k,n}^{(j)})$, $\alpha_k(\tilde{\mathbf{a}}_{k,n}^{(j)}, 1)$, and $\alpha_{k,n}^{(j)}$, the message $\gamma_k^{(j)}(\mathbf{x}_n)$ related to the agent is calculated as

$$\gamma_k^{(j)}(\mathbf{x}_n) = \sum_{c_{k,n}^{(j)}=0}^{M_n^{(j)}} \eta(c_{k,n}^{(j)}) \int \alpha_k(\tilde{\mathbf{a}}_{k,n}^{(j)}, 1) g(\mathbf{x}_n, \tilde{\mathbf{a}}_{k,n}^{(j)}, 1, c_{k,n}^{(j)}; \mathbf{z}_n^{(j)}) d\tilde{\mathbf{a}}_{k,n}^{(j)} + \eta(c_{k,n}^{(j)}=0) \alpha_{k,n}^{(j)}. \quad (41)$$

5) *Measurement update for legacy PFs:* Similarly, the messages $\gamma(\tilde{\mathbf{a}}_{k,n}^{(j)}, \tilde{r}_{k,n}^{(j)})$ related to the legacy PFs are calculated as

$$\gamma(\tilde{\mathbf{a}}_{k,n}^{(j)}, 1) = \sum_{c_{k,n}^{(j)}=0}^{M_n^{(j)}} \eta(c_{k,n}^{(j)}) \int \alpha(\mathbf{x}_n) g(\mathbf{x}_n, \tilde{\mathbf{a}}_{k,n}^{(j)}, 1, c_{k,n}^{(j)}; \mathbf{z}_n^{(j)}) d\mathbf{x}_n \quad (42)$$

$$\gamma_{k,n}^{(j)} \triangleq \gamma(\tilde{\mathbf{a}}_{k,n}^{(j)}, 0) = \eta(c_{k,n}^{(j)}=0). \quad (43)$$

6) *Measurement update for new PFs*: Finally, the messages $\phi(\check{\mathbf{a}}_{m,n}^{(j)}, \check{r}_{m,n}^{(j)})$ related to the new PFs are calculated as

$$\phi(\check{\mathbf{a}}_{m,n}^{(j)}, 1) = \varsigma(b_{m,n}^{(j)} = 0) \int \alpha(\mathbf{x}_n) h(\mathbf{x}_n, \check{\mathbf{a}}_{m,n}^{(j)}, 1, 0; \mathbf{z}_n^{(j)}) d\mathbf{x}_n \quad (44)$$

$$\phi_{m,n}^{(j)} \triangleq \phi(\check{\mathbf{a}}_{k,n}^{(j)}, 0) = \sum_{\substack{b_{m,n}^{(j)} = 0}}^{K_{n-1}^{(j)}} \varsigma(b_{m,n}^{(j)}). \quad (45)$$

Once all these messages have been calculated, the beliefs approximating the desired marginal posterior pdfs are obtained. The belief for the agent state is given, up to a constant normalization factor, by

$$q(\mathbf{x}_n) \propto \alpha(\mathbf{x}_n) \prod_{j=1}^J \prod_{k \in \mathcal{K}_{n-1}^{(j)}} \gamma_k^{(j)}(\mathbf{x}_n). \quad (46)$$

This belief after normalization provides an approximation of the marginal posterior pdf $f(\mathbf{x}_n | \mathbf{z}_{1:n})$, and it is used instead of $f(\mathbf{x}_n | \mathbf{z}_{1:n})$ in (27). Furthermore, the beliefs $\tilde{q}(\tilde{\mathbf{a}}_{k,n}^{(j)}, \tilde{r}_{k,n}^{(j)})$ for the augmented states of the legacy PFs, $\tilde{\mathbf{y}}_{k,n}^{(j)} = [\tilde{\mathbf{a}}_{k,n}^{(j)\top} \ \tilde{r}_{k,n}^{(j)}]^\top$, are calculated as

$$\tilde{q}(\tilde{\mathbf{a}}_{k,n}^{(j)}, 1) \propto \alpha_k(\tilde{\mathbf{a}}_{k,n}^{(j)}, 1) \gamma(\tilde{\mathbf{a}}_{k,n}^{(j)}, 1), \quad \tilde{q}_{k,n}^{(j)} \triangleq \tilde{q}(\tilde{\mathbf{a}}_{k,n}^{(j)}, 0) \propto \alpha_{k,n}^{(j)} \gamma_{k,n}^{(j)}, \quad (47)$$

and the beliefs $\check{q}(\check{\mathbf{a}}_{m,n}^{(j)}, \check{r}_{m,n}^{(j)})$ for the augmented states of the new PFs, $\check{\mathbf{y}}_{m,n}^{(j)} = [\check{\mathbf{a}}_{m,n}^{(j)\top} \ \check{r}_{m,n}^{(j)}]^\top$, are calculated as

$$\check{q}(\check{\mathbf{a}}_{m,n}^{(j)}, 1) \propto \phi(\check{\mathbf{a}}_{m,n}^{(j)}, 1), \quad \check{q}_{m,n}^{(j)} \triangleq \check{q}(\check{\mathbf{a}}_{m,n}^{(j)}, 0) \propto \phi_{m,n}^{(j)}. \quad (48)$$

In particular, $\tilde{q}(\tilde{\mathbf{a}}_{k,n}^{(j)}, 1)$ and $\check{q}(\check{\mathbf{a}}_{m,n}^{(j)}, 1)$ approximate the marginal posterior pdf $f(\mathbf{a}_{k',n}^{(j)}, r_{k',n}^{(j)} = 1 | \mathbf{z}_{1:n})$, where $k' \in \mathcal{K}_{n-1}^{(j)} \cup \mathcal{M}_n^{(j)}$ (assuming an appropriate index mapping between k and m on the one hand and k' on the other), and they are used in (28) and (29), (30).

An exact calculation of the various messages and beliefs by direct evaluation of the expressions presented above is infeasible. An efficient approximate calculation can be based on the sequential Monte Carlo (particle-based) implementation approach introduced in [31], [41]. In our case, the sequential Monte Carlo implementation uses a “stacked state” [41] comprising the agent state and the PF states. The resulting complexity scales only linearly in the number of particles.

VI. STATE PROPAGATION FOR UNDETECTED FEATURES

In parallel to, and in support of, the BP-based detection and estimation algorithm, we use a “zero-measurement” PHD filter in order to propagate information about features that potentially

exist but did not generate any measurement yet. Such features will be termed *undetected features*. in what follows. A similar strategy was previously introduced in the context of MTT [26], [34]. This propagation of information about undetected features enables the calculation of the intensity function of newly detected features, $\lambda_n^n(\mathbf{a}_{\cdot,n}^{(j)}|\mathbf{x}_n) = \mu_{n,n}^{(j)} f_{n,n}(\mathbf{a}_{\cdot,n}^{(j)}|\mathbf{x}_n)$, for all PAs j at time n . Note that $\lambda_n^n(\check{\mathbf{a}}_{m,n}^{(j)}|\mathbf{x}_n)$ occurs in $h(\mathbf{x}_n, \check{\mathbf{a}}_{m,n}^{(j)}, 1, 0; \mathbf{z}_n^{(j)})$ in (24), which is needed in the measurement evaluation and measurement update steps for new PFs (see Section V-B). We will first review the concept of a Poisson random finite set (RFS), which underlies the PHD filter.

A. RFS Basics

An RFS [27], also known as a simple finite point process [42], is a set-valued random variable $\mathbf{X} = \{\mathbf{x}^{(1)}, \dots, \mathbf{x}^{(k)}\}$. The elements of \mathbf{X} are random vectors $\mathbf{x}^{(i)} \in \mathbb{R}^{N_x}$; they are unordered and their number $k = |\mathbf{X}| \in \mathbb{N}_0$ —i.e., the cardinality of \mathbf{X} —is random. The realizations of \mathbf{X} , $\mathcal{X} = \{\mathbf{x}^{(1)}, \dots, \mathbf{x}^{(k)}\}$, are finite sets of vectors $\mathbf{x}^{(1)}, \dots, \mathbf{x}^{(k)} \in \mathbb{R}^{N_x}$. Within the FISST framework [27], an RFS \mathbf{X} can be described by its pdf $f_{\mathbf{X}}(\mathcal{X})$, briefly denoted $f(\mathcal{X})$. The pdf evaluated for a realization $\mathcal{X} = \{\mathbf{x}^{(1)}, \dots, \mathbf{x}^{(k)}\}$ is given by $f(\mathcal{X}) = f(\{\mathbf{x}^{(1)}, \dots, \mathbf{x}^{(k)}\}) = k! \rho(k) f_k(\mathbf{x}^{(1)}, \dots, \mathbf{x}^{(k)})$. Here, $\rho(k) \triangleq \Pr\{|\mathbf{X}| = k\}$ is the pmf of the cardinality $k = |\mathbf{X}|$, which is termed the cardinality distribution, and $f_k(\mathbf{x}^{(1)}, \dots, \mathbf{x}^{(k)})$ is the joint pdf of the random vectors $\mathbf{x}^{(1)}, \dots, \mathbf{x}^{(k)}$, which is required to be invariant to a permutation of its arguments $\mathbf{x}^{(i)}$.

An important special RFS is the Poisson RFS. The elements of a Poisson RFS \mathbf{X} are iid with some “spatial pdf” $f(\mathbf{x})$. Thus, for cardinality $|\mathcal{X}| = k$, $f_k(\mathbf{x}^{(1)}, \dots, \mathbf{x}^{(k)}) = \prod_{i=1}^k f(\mathbf{x}^{(i)}) = \prod_{\mathbf{x} \in \mathcal{X}} f(\mathbf{x})$. The cardinality $k = |\mathbf{X}|$ is Poisson distributed, i.e., $\rho(k) = e^{-\mu} \mu^k / k!$, $k \in \mathbb{N}_0$, where μ is the mean of k . The pdf of \mathbf{X} follows as $f(\mathcal{X}) = e^{-\mu} \prod_{\mathbf{x} \in \mathcal{X}} \mu f(\mathbf{x})$. The Poisson RFS is also fully characterized by its intensity function or PHD, which is given by $\lambda(\mathbf{x}) = \mu f(\mathbf{x})$.

B. Zero-Measurement PHD Filter

The PHD filter is a popular technique for tracking an RFS [27]. In the PHD filter, the state is modeled as a Poisson RFS. The original PHD filter [27] propagates the intensity functions of both the detected and undetected features. In order to keep the RFS within the class of Poisson RFSs, an approximation is performed in the update step of the PHD filter. In [26], [34], a PHD filter that propagates only the intensity function of the undetected features is introduced. In this filter, which we will term a zero-measurement PHD filter, the propagated RFS remains within the class of Poisson RFSs without any approximation. In the proposed

SLAM algorithm, the zero-measurement PHD filter complements the BP-based algorithm in Section V-B because it propagates information about undetected features whereas the BP-based algorithm propagates information about detected features. We assume that at the initial time $n = 1$, the state of the undetected features for PA j is a Poisson RFS with intensity function $\lambda^u(\mathbf{a}_{\cdot,1}^{(j)})$. In practice, $\lambda^u(\mathbf{a}_{\cdot,1}^{(j)})$ can be chosen constant on the region of interest (ROI), with the integral of $\lambda^u(\mathbf{a}_{\cdot,1}^{(j)})$ over the ROI chosen equal to the expected number of features in the ROI. Using a zero-measurement PHD filter, state propagation for the undetected features amounts to propagating the intensity function of the Poisson RFS (i.e., $\lambda^u(\mathbf{a}_{\cdot,n-1}^{(j)}) \rightarrow \lambda^u(\mathbf{a}_{\cdot,n}^{(j)})$). This propagation consists of a prediction step and an update step.

1) *Prediction Step*: In the prediction step, which is identical to that of the original PHD filter [27], the preceding intensity function $\lambda^u(\mathbf{a}_{\cdot,n-1}^{(j)})$ is converted into a “predicted intensity function” $\lambda_{n|n-1}^u(\mathbf{a}_{\cdot,n}^{(j)})$ according to

$$\lambda_{n|n-1}^u(\mathbf{a}_{\cdot,n}^{(j)}) = P_s \int f(\mathbf{a}_{\cdot,n}^{(j)} | \mathbf{a}_{\cdot,n-1}^{(j)}) \lambda_{n-1}^u(\mathbf{a}_{\cdot,n-1}^{(j)}) d\mathbf{a}_{\cdot,n-1}^{(j)} + \lambda^b(\mathbf{a}_{\cdot,n}^{(j)}), \quad (49)$$

where $f(\mathbf{a}_{\cdot,n}^{(j)} | \mathbf{a}_{\cdot,n-1}^{(j)})$ is the state-transition pdf of the undetected feature state. Here, $\lambda^b(\mathbf{a}_{\cdot,n}^{(j)})$ is the intensity function of a Poisson RFS that models the birth of new features. In the SLAM context, it may be reasonable to set $\lambda^b(\mathbf{a}_{\cdot,n}^{(j)}) = 0$, which expresses the assumption that the indoor geometry does not change during the mapping process. From $\lambda_{n|n-1}^u(\mathbf{a}_{\cdot,n}^{(j)})$, the conditional pdf $f_n^u(\mathbf{a}_{\cdot,n}^{(j)} | \mathbf{x}_n)$ for newly detected features for PA j is obtained as [26]

$$f_n^u(\mathbf{a}_{\cdot,n}^{(j)} | \mathbf{x}_n) = \frac{P_d^{(j)}(\mathbf{x}_n, \mathbf{a}_{\cdot,n}^{(j)}) \lambda_{n|n-1}^u(\mathbf{a}_{\cdot,n}^{(j)})}{\int P_d^{(j)}(\mathbf{x}_n, \mathbf{a}_{\cdot,n}^{(j) \prime}) \lambda_{n|n-1}^u(\mathbf{a}_{\cdot,n}^{(j) \prime}) d\mathbf{a}_{\cdot,n}^{(j) \prime}}, \quad (50)$$

where $P_d^{(j)}(\mathbf{x}_n, \mathbf{a}_{\cdot,n}^{(j)})$ is the detection probability of the undetected feature state for PA j . Furthermore, the mean number of newly detected features is given by $\mu_{n,n}^{(j)} = \int \int P_d^{(j)}(\mathbf{x}_n, \mathbf{a}_{\cdot,n}^{(j)}) \times \lambda_{n|n-1}^u(\mathbf{a}_{\cdot,n}^{(j)}) \alpha(\mathbf{x}_n) d\mathbf{a}_{\cdot,n}^{(j)} d\mathbf{x}_n$, with $\alpha(\mathbf{x}_n)$ according to (31). As mentioned earlier, $f_n^u(\mathbf{a}_{\cdot,n}^{(j)} | \mathbf{x}_n)$ and $\mu_{n,n}^{(j)}$ are needed in the measurement evaluation and measurement update steps for new PFs described in Section V-B.

2) *Update Step*: In the update step, the predicted intensity function $\lambda_{n|n-1}^u(\mathbf{a}_{\cdot,n}^{(j)})$ is converted into the new (updated) intensity function $\lambda^u(\mathbf{a}_{\cdot,n}^{(j)})$ according to [26], [34]

$$\lambda^u(\mathbf{a}_{\cdot,n}^{(j)}) = (1 - P_d^{(j)}(\mathbf{a}_{\cdot,n}^{(j)})) \lambda_{n|n-1}^u(\mathbf{a}_{\cdot,n}^{(j)}), \quad (51)$$

where $P_d^{(j)}(\mathbf{a}_{\cdot,n}^{(j)}) = \int P_d^{(j)}(\mathbf{x}_n, \mathbf{a}_{\cdot,n}^{(j)}) \alpha(\mathbf{x}_n) d\mathbf{x}_n$. We note that this update relation is identical to that of the original PHD filter [27] for the case where no measurements are available. The

intensity function $\lambda^u(\mathbf{a}_{\cdot,n}^{(j)})$ represents essentially “negative information” in the sense that for $\lambda^b(\mathbf{a}_{\cdot,n}^{(j)}) = 0$, $\lambda^u(\mathbf{a}_{\cdot,n}^{(j)})$ is high in those parts of the ROI that have not been explored by the mobile agent yet, and for $\lambda^b(\mathbf{a}_{\cdot,n}^{(j)}) > 0$, it is high in those parts of the ROI that have not been explored for some time. The expressions (49) and (51) are calculated by using a sequential Monte Carlo implementation, similarly to [35].

VII. EXPERIMENTAL RESULTS

To analyze the performance of the proposed algorithm, we apply it to synthetic and real measurement data within two-dimensional (2-D) scenarios.

A. Analysis Setup

1) *State-Evolution Model*: The agent’s state-transition pdf $f(\mathbf{x}_n | \mathbf{x}_{n-1})$, with $\mathbf{x}_n = [\mathbf{p}_n^T \mathbf{v}_n^T]^T$, is defined by a linear constant-velocity motion model [43]. This model involves a driving process \mathbf{w}_n that is independent across n , zero-mean, and Gaussian with covariance matrix $\mathbf{R}_w = \sigma_w^2 \mathbf{I}_2$, where $\sigma_w = 0.0033$ m/step and \mathbf{I}_2 denotes the 2×2 identity matrix. The PFs are static, i.e., the state-transition pdfs are given by $f(\tilde{\mathbf{a}}_{k,n}^{(j)} | \mathbf{a}_{k,n-1}^{(j)}) = \delta(\tilde{\mathbf{a}}_{k,n}^{(j)} - \mathbf{a}_{k,n-1}^{(j)})$, where $\delta(\cdot)$ is the Dirac delta function. However, in our implementation of the proposed algorithm, for the sake of numerical stability, we introduced a small driving process in the PF state-evolution model. Accordingly, the state evolution is modeled as $\tilde{\mathbf{a}}_{k,n}^{(j)} = \mathbf{a}_{k,n-1}^{(j)} + \boldsymbol{\omega}_{k,n}^{(j)}$, where $\boldsymbol{\omega}_{k,n}^{(j)}$ is independent across k , n , and j , zero-mean, and Gaussian with covariance matrix $\boldsymbol{\Omega}_{k,n}^{(j)} = \sigma_a^2 \mathbf{I}_2$, where $\sigma_a = 0.015$ m.

2) *Measurement Model*: We consider scalar range measurements $z_{m,n}^{(j)}$, which are modeled as

$$z_{m,n}^{(j)} = \|\mathbf{p}_n - \mathbf{a}_{k,n}^{(j)}\| + \nu_{m,n}^{(j)}. \quad (52)$$

Here, the measurement noise $\nu_{m,n}^{(j)}$ is independent across m , n , and j , zero-mean, and Gaussian with variance $\sigma_{m,n}^{(j)2}$. Note that the measurement model (52) determines the likelihood function factors $f(z_{m,n}^{(j)} | \mathbf{x}_n, \tilde{\mathbf{a}}_{k,n}^{(j)})$ and $f(z_{m,n}^{(j)} | \mathbf{x}_n, \check{\mathbf{a}}_{m,n}^{(j)})$ in (14). We emphasize that in contrast to usual SLAM setups [2], our measurement model is solely based on MPC delays, i.e., it does not exploit bearing information or information derived from inertial measurement unit sensors. Inclusion of such information would further improve the robustness of our approach.

3) *Common Simulation Parameters*: The following implementation parameters are used for both synthetic and real measurements (parameters that are chosen differently for synthetic and real measurements will be described in Sections VII-B and VII-C). We use the floor plan shown

in Fig. 1, with two static PAs at positions $\mathbf{a}_{1,n}^{(1)}$ and $\mathbf{a}_{1,n}^{(2)}$. The false alarm pdf $f_{\text{FA}}(z_{m,n}^{(j)})$ is uniform on [0m, 30m]. The survival probability is $P_s = 0.999$. The birth intensity function $\lambda^b(\mathbf{a}_{\cdot,n}^{(j)})$ is uniform on the ROI, which is a circular disk of radius 30m around the center of the floor plan shown in Fig. 1. Thus, $\lambda^b(\mathbf{a}_{\cdot,n}^{(j)}) = \mu_b/(2\pi(30\text{m})^2)$, with the mean number of newborn features $\mu_b = 10^{-4}$. Similarly, the initial undetected feature intensity is uniform on the ROI, i.e., $\lambda^u_1(\mathbf{a}_{\cdot,1}^{(j)}) = \mu_{n,1}^{(j)}/(2\pi(30\text{m})^2)$, with the initial mean number of undetected features $\mu_{n,1}^{(j)} = 10$. The detection threshold is $P_{\text{det}} = 0.5$, and the pruning threshold is $P_{\text{prun}} = 10^{-4}$. Our implementation of the proposed algorithm uses a sequential importance resampling particle filter scheme that follows the implementations in [31], [41]. The particles for the initial states of the two PAs are drawn from the 2-D Gaussian distributions $\mathcal{N}(\mathbf{a}_{1,1}^{(j)}, \sigma_{a,1}^2 \mathbf{I}_2)$, where $\mathbf{a}_{1,1}^{(j)}$ is the position of PA $j \in \{1, 2\}$ and $\sigma_{a,1} = 0.01\text{m}$. The particles for the initial agent state are drawn from a 4-D uniform distribution with center $[\mathbf{p}_1^T \ 0 \ 0]^T$, where \mathbf{p}_1 is the starting position of the agent trajectory, and support of each component about the respective center given by $[-0.1, 0.1]$ (in m for the position and m/step for the velocity). The number P of message passing iterations for DA is limited by the termination condition $[\sum_{k \in \mathcal{K}_{n-1}^{(j)}} \sum_{m \in \mathcal{M}_n^{(j)}} (\nu_{m \rightarrow k}^{(p)}(c_{k,n}^{(j)}) - \nu_{m \rightarrow k}^{(p-1)}(c_{k,n}^{(j)}))^2]^{1/2} < 10^{-7}$ (cf. (38)) or by the maximum number $P_{\text{max}} = 1000$.

B. Results for Synthetic Measurements

For our simulations based on synthetic measurements, we used the common simulation parameters described above and, in addition, measurement noise standard deviation $\sigma_{m,n}^{(j)} = 0.1\text{ m}$. We considered three different parameter settings dubbed SLAM 1, SLAM 2, and SLAM 3. In SLAM 1 and SLAM 2, we used detection probability $P_d^{(j)}(\mathbf{x}_n, \mathbf{a}_{k,n}^{(j)}) = P_d = 0.95$ and mean number of false alarms $\mu_{\text{FA}}^{(j)} = 1$. The posterior pdfs of the state of the mobile agent, of the states of legacy PFs, and of the states of new PFs were each represented by 100.000 (SLAM 1) or by 30.000 (SLAM 2) particles.² In SLAM 3, we used $P_d = 0.5$ and $\mu_{\text{FA}}^{(j)} = 2$ to analyze the robustness of the proposed algorithm in poor radio signal conditions; for this parameter setting, the agent state and the PF states were each represented by 100.000 particles. We performed 100 simulation runs. In each simulation run, we generated with detection probability P_d noisy ranges

²The number of particles could be reduced significantly if, e.g., the MPCs' AoAs were used in addition to the range (delay) measurements, since this would strongly decrease the effective support regions of the posterior pdfs. The number of particles could also be reduced by performing an adaptive adjustment of the detection probability P_d as in [22]. Since the complexity of the proposed algorithm scales only linearly with the number of particles, the runtime of a MATLAB implementation on an Intel i7-6820HQ CPU is still below 0.4s per time step n even for these high numbers of particles. Further results about the runtime versus the number of features, the number of measurements, and the number of PAs can be found in [31].

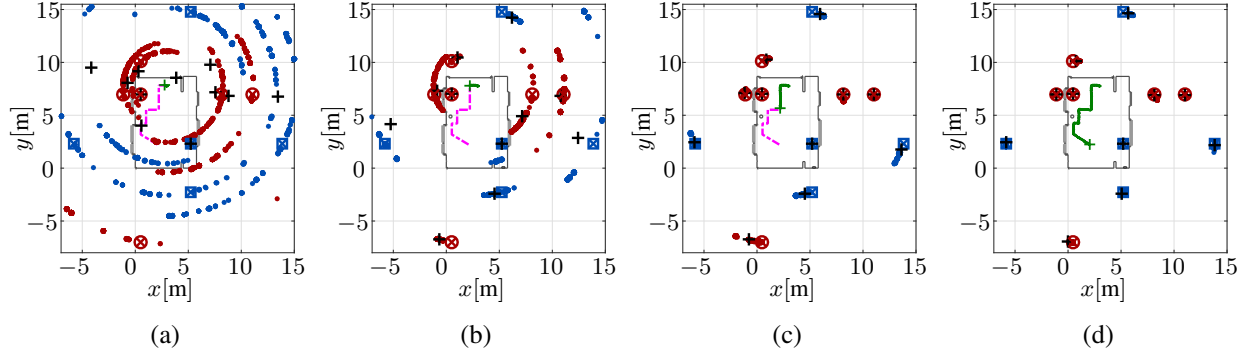


Fig. 3: Illustration of particle convergence for synthetic measurements. Particles representing the posterior pdfs of the state of the mobile agent (green) and of the states of the detected PFs (red for PA 1, blue for PA 2) are shown at (a) $n=30$, (b) $n=90$, (c) $n=300$, and (d) $n=900$. The red circle-crosses and blue square-crosses indicate the positions of, respectively, PA 1 and PA 2 along with the corresponding VA positions (cf. Fig 1). The black crosses represent the estimated positions of the detected PFs.

$z_{m,n}^{(j)}$ according to (52). Evaluation of (52) was based on the fixed PA positions $\mathbf{a}_{1,n}^{(1)}$, $\mathbf{a}_{1,n}^{(2)}$ and the fixed VA positions $\mathbf{a}_{l,n}^{(j)} \in \mathbb{R}^2$, $l = 2, \dots, L_n^{(j)}$ for $j = 1, 2$ (shown in Fig. 1), where $L_n^{(1)} = 6$ and $L_n^{(2)} = 5$ are the numbers of features (PA plus VAs). In addition, false alarm measurements $z_{m,n}^{(j)}$ were generated according to the false alarm parameters described above.

For one exemplary simulation run, Fig. 3 illustrates the convergence of the posterior pdfs of the PF positions to the true feature (PA and VA) positions by displaying the respective particles at times $n = 30, 90, 300, 900$. These results demonstrate that the proposed algorithm is able to cope with highly multimodal distributions and with measurements conveying only very limited information at each time step (since only range measurements are used).

Fig. 4 shows the root mean square error (RMSE) of the estimated time-varying agent position, the average numbers of detected PFs for the two PAs, and the mean optimal subpattern assignment (MOSPA) errors [44] for the two PAs, all displayed versus time n . These results were obtained by averaging over the 100 simulation runs. The MOSPA errors are based on the Euclidean metric and use cutoff parameter 10m and order parameter 1 [44]. It can be seen in Fig. 4(a) that the average agent position RMSE is below 0.13m for all parameters settings. The sudden increase of the RMSE around time $n=100$ can be explained by the sharp 90-degree turn of the mobile agent at time $n=100$, together with the range-only measurement model; note that the latter leads to a slow convergence of the multimodal posterior distributions of the PF states. The average numbers of detected PFs for SLAM 1 and SLAM 2 are seen in Figs. 4(b), (c) to be effectively equal to the respective true numbers of features $L_n^{(1)} = 6$ and $L_n^{(2)} = 5$. For SLAM 3, the average

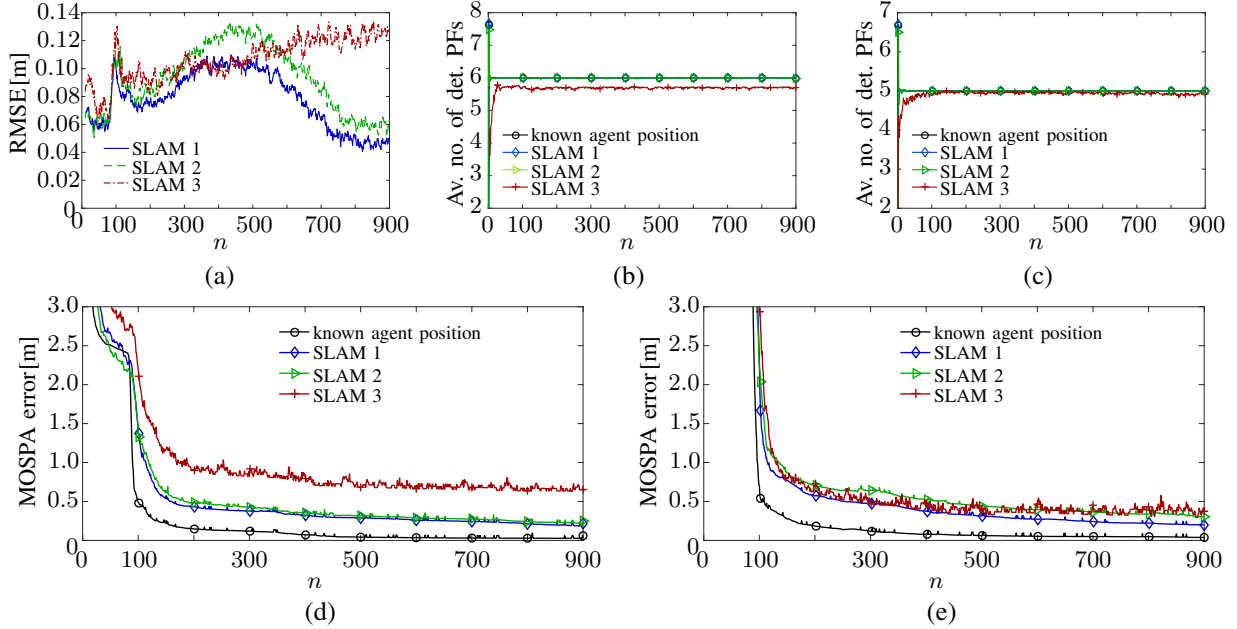


Fig. 4: Results for synthetic measurements: (a) Average agent position RMSE, (b) and (c) average number of detected PFs for PA 1 and 2, respectively, (d) and (e) MOSPA error for PA 1 and 2, respectively. The curves labeled “known agent position” show the performance for the case where the agent position is known. The parameter settings (SLAM 1, SLAM 2, and SLAM 3) corresponding to the various curves are specified in the main text. Note that in (b) and (c) the curves labeled “known agent position,” “SLAM 1,” and “SLAM 2” coincide.

number of detected PFs is slightly below the true numbers of features, which can be explained by the low detection probability $P_d = 0.5$ and the high mean number of false alarms $\mu_{\text{FA}}^{(j)} = 2$ relative to the true numbers of features $L_n^{(1)} = 6$ and $L_n^{(2)} = 5$. However, the performance of the algorithm is still quite good, which suggests that the algorithm has a high level of robustness. The MOSPA errors for SLAM 1 and SLAM 2 are seen in Figs. 4(d), (e) to decrease with time until they are ultimately below 0.2m for both PAs. In general, the RMSE and MOSPA errors for SLAM 3 are somewhat larger. As a performance benchmark, Figs. 4(b)–(e) also show the average number of detected PFs and the MOSPA errors that would be obtained for parameter setting SLAM 1 if the agent position was known at all times.

C. Results for Real Measurements

For experiments using real measurements, we chose $P_d^{(j)}(x_n, a_{k,n}^{(j)}) = P_d = 0.6$ and $\mu_{\text{FA}}^{(j)} = 2$. This accounts for the fact that the diffuse multipath existing in indoor environments causes the preliminary signal analysis stage to detect features with a lower probability and to produce false detections (false alarms) with a higher probability. The measurements were taken from the seminar room scenario previously used in [22], [45]. They correspond to five closely spaced

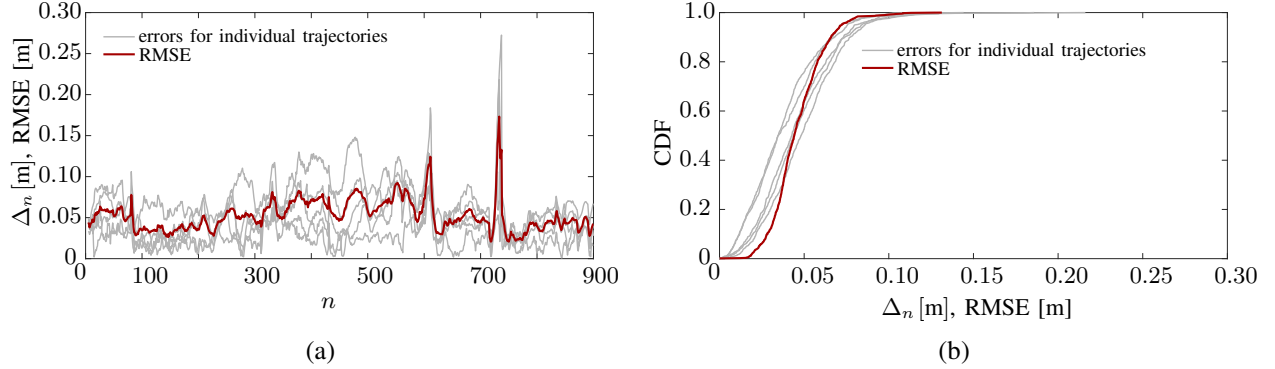


Fig. 5: Results for real measurements: (a) Agent position estimation errors Δ_n for the five individual trajectories and RMSE (averaged over the five trajectories), (b) empirical CDFs of Δ_n for the five individual trajectories and of the RMSE for all 4500 radio signals.

parallel trajectories each consisting of 900 agent positions with a 1cm spacing, resulting in a total number of 4500 agent positions. The magenta line in Fig. 1 represents one of the five trajectories. More details about the measurements can be found in [45]. At each agent position, the agent transmitted an ultra-wideband signal, which was received by the two static PAs. This signal was measured using an M-sequence correlative channel sounder with frequency range 3–10GHz and antennas with an approximately uniform radiation pattern in the azimuth plane and zeros in the floor and ceiling directions. Within the measured band, the actual signal band was selected by a filter with raised-cosine impulse response $s(t)$ with a roll-off factor of 0.5, a two-sided 3-dB bandwidth of 2GHz, and a center frequency of 7GHz. From the measured signals, the range measurements $z_{m,n}^{(j)} = c\hat{\tau}_{m,n}^{(j)}$ constituting the input to the proposed algorithm were derived by means of a snapshot-based SISO SAGE algorithm [17] for estimating the delays $\tau_{m,n}^{(j)}$ and complex amplitudes $\alpha_{m,n}^{(j)}$ of the MPCs (cf. (1)). In this method, the maximum number of estimated MPCs for each PA j was defined as $M_{n,\max}^{(j)} = 15$. Estimates of the range variances $\sigma_{m,n}^{(j)2}$ (cf. (52)) were determined from the estimated complex amplitudes as described in [22], [45]. The pdfs of the states were represented by 100.000 particles each.

Fig. 5(a) shows the agent position estimation errors $\Delta_n \triangleq \|\hat{\mathbf{p}}_n - \mathbf{p}_n\|$ obtained for the five individual trajectories versus time n , along with the RMSE (averaged over the five trajectories). Fig. 5(b) shows the empirical cumulative distribution function (CDF) of Δ_n , individually for the five trajectories, and the CDF of the RMSE for the total set of 4500 radio signals. It can be seen that the individual CDFs are very close to 1 already at Δ_n equal to 12cm or even less. The maximum Δ_n is below 22cm in all cases. Moreover, the RMSE is below 13.5cm in all cases

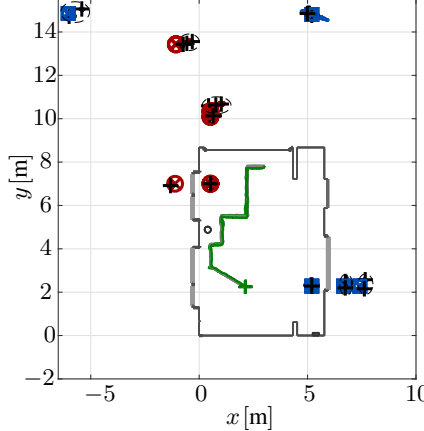


Fig. 6: Results for real measurements: Particles representing the posterior pdfs of the states of the mobile agent (green) and of the detected PFs (red for PA 1, blue for PA 2). The red circle-crosses and blue square-crosses indicate the positions of, respectively, PA 1 and PA 2 along with the corresponding geometrically expected VA positions (cf. Fig 1). The black crosses represent the estimated positions of the detected PFs. The dashed black ellipses group PF positions that can be associated with the geometrically expected position of one VA.

and below 7.2cm in 90% of all cases.³

Fig. 6 shows the particles representing the posterior pdfs of the states of the mobile agent and of the detected PFs and the MMSE estimates of the positions of the detected PFs for the five trajectories. All estimated PF positions can be associated with geometrically expected VA positions. This demonstrates that the proposed algorithm is able to leverage position-related information contained in the radio signals for accurate and robust localization. The rather low number of detected PFs can be attributed to two main reasons. First, the used snapshot-based SISO channel estimator is severely challenged by the overlap of MPCs and by the interfering diffuse multipath component, even though ultra-wideband signals are employed. These effects lead to a larger fading and, in turn, a lower signal-to-interference-and-noise ratio [36]. Second, the complex structure of an indoor environment leads to many different MPCs, whose detectability depends strongly on the agent position. The number of detected PFs could be increased by using an adaptive adjustment of the detection probabilities [22].

VIII. CONCLUSIONS AND FUTURE PERSPECTIVES

We have proposed a radio signal based SLAM algorithm with probabilistic DA. The underlying system model describes specular MPCs in terms of VAs, whose positions are unknown and

³The lower values of Δ_n (below 7.2cm in all cases and below 3.5cm in 90% of all cases) obtained by the SLAM algorithm in [22] is due to an adaptive adjustment of the detection probability P_d .

possibly time-varying. A major complication in radio signal based SLAM is the DA problem, i.e., the fact that the association between MPCs and VAs is unknown. To address this challenge, we modeled the entire SLAM problem including probabilistic DA in a Bayesian framework and represented the factorization structure of the joint posterior distribution by a factor graph. We then applied the BP scheme for approximate marginalization of the joint posterior distribution. This approach allowed the incorporation of an efficient BP algorithm for probabilistic DA that was originally proposed for multitarget tracking [30], [31]. Our factor graph extends that of [22] by the states of new potential features and undetected features. The intensity functions of the latter are tracked by a “zero-measurement” PHD filter, which allows an improved initialization of the positions of new potential features.

Simulation results using synthetic data showed that the proposed SLAM algorithm estimates the time-varying agent position with high accuracy. Moreover, it determines the feature map with a low MOSPA error, which means that it almost always detects the correct number of features and estimates their positions with high accuracy. An extensive experimental analysis using real ultra-wideband radio signals in an indoor environment showed that our algorithm performs similarly well in real-world scenarios; the agent position error was observed to be below 22cm for 100% and below 7.2cm for 90% of all measurements.

A promising direction for future research is an extension of our algorithm that uses the complex MPC amplitudes for estimating and tracking the detection probabilities and measurement noise variances of the sensors. The algorithm can also be extended to exploit further MPC parameters, such as AoAs and AoDs, and to track additional types of features, such as scatter points. Finally, modifications of our algorithm for operation in an unsynchronized sensor network and for a distributed (decentralized) mode of operation would be theoretically and practically interesting.

REFERENCES

- [1] H. Durrant-Whyte and T. Bailey, “Simultaneous localization and mapping: Part I,” *IEEE Robot. Autom. Mag.*, vol. 13, no. 2, pp. 99–110, Jun. 2006.
- [2] S. Thrun, W. Burgard, and D. Fox, *Probabilistic Robotics (Intelligent Robotics and Autonomous Agents)*. Cambridge, MA, USA: MIT Press, 2005.
- [3] R. Di Taranto, S. Muppirisetty, R. Raulefs, D. Slock, T. Svensson, and H. Wymeersch, “Location-aware communications for 5G networks: How location information can improve scalability, latency, and robustness of 5G,” *IEEE Signal Process. Mag.*, vol. 31, no. 6, pp. 102–112, Nov 2014.

- [4] K. Witrisal, P. Meissner, E. Leitinger, Y. Shen, C. Gustafson, F. Tufvesson, K. Haneda, D. Dardari, A. F. Molisch, A. Conti, and M. Z. Win, "High-accuracy localization for assisted living: 5G systems will turn multipath channels from foe to friend," *IEEE Signal Process. Mag.*, vol. 33, no. 2, pp. 59–70, Mar. 2016.
- [5] D. Dardari, P. Closas, and P. M. Djurić, "Indoor tracking: Theory, methods, and technologies," *IEEE Trans. Veh. Technol.*, vol. 64, no. 4, pp. 1263–1278, Apr. 2015.
- [6] F. Guidi, A. Guerra, and D. Dardari, "Personal mobile radars with millimeter-wave massive arrays for indoor mapping," *IEEE Trans. Mobile Comput.*, vol. 15, no. 6, pp. 1471–1484, Jun. 2016.
- [7] E. Leitinger, F. Meyer, P. Meissner, K. Witrisal, and F. Hlawatsch, "Belief propagation based joint probabilistic data association for multipath-assisted indoor navigation and tracking," in *Proc. ICL-GNSS-16*, Barcelona, Spain, Jun. 2016.
- [8] M. Dissanayake, P. Newman, S. Clark, H. Durrant-Whyte, and M. Csorba, "A solution to the simultaneous localization and map building (SLAM) problem," *IEEE Trans. Robot. Autom.*, vol. 17, no. 3, pp. 229–241, Jun. 2001.
- [9] J. Mullane, B.-N. Vo, M. Adams, and B.-T. Vo, "A random-finite-set approach to Bayesian SLAM," *IEEE Trans. Robot.*, vol. 27, no. 2, pp. 268–282, Apr. 2011.
- [10] M. Lundgren, L. Svensson, and L. Hammarstrand, "Variational Bayesian expectation maximization for radar map estimation," *IEEE Trans. Signal Process.*, vol. 64, no. 6, pp. 1391–1404, Mar. 2016.
- [11] M. Fatemi, L. Svensson, L. Hammarstrand, and M. Lundgren, "Variational Bayesian EM for SLAM," in *Proc. IEEE CAMSAP-15*, Cancun, Mexico, Dec. 2015, pp. 501–504.
- [12] H. Deusch, S. Reuter, and K. Dietmayer, "The labeled multi-Bernoulli SLAM filter," *IEEE Signal Process. Lett.*, vol. 22, no. 10, pp. 1561–1565, Oct. 2015.
- [13] M. Fatemi, K. Granström, L. Svensson, F. J. R. Ruiz, and L. Hammarstrand, "Poisson multi-Bernoulli mapping using Gibbs sampling," *IEEE Trans. Signal Process.*, vol. 65, no. 11, pp. 2814–2827, Jun. 2017.
- [14] E. Leitinger, P. Meissner, M. Lafer, and K. Witrisal, "Simultaneous localization and mapping using multipath channel information," in *Proc. IEEE ICC-15*, London, UK, Jun. 2015, pp. 754–760.
- [15] C. Gentner, T. Jost, W. Wang, S. Zhang, A. Dammann, and U. C. Fiebig, "Multipath assisted positioning with simultaneous localization and mapping," *IEEE Trans. Wireless Commun.*, vol. 15, no. 9, pp. 6104–6117, Sep. 2016.
- [16] M. Zhu, J. Vieira, Y. Kuang, K. Astrom, A. Molisch, and F. Tufvesson, "Tracking and positioning using phase information from estimated multi-path components," in *Proc. IEEE ICCW-15*, Jun. 2015, pp. 712–717.
- [17] B. Fleury, M. Tschudin, R. Heddergott, D. Dahlhaus, and K. Ingeman Pedersen, "Channel parameter estimation in mobile radio environments using the SAGE algorithm," *IEEE J. Sel. Areas Commun.*, vol. 17, no. 3, pp. 434–450, Mar. 1999.
- [18] A. Richter, "Estimation of Radio Channel Parameters," Ph.D. dissertation, Ilmenau University of Technology, 2005.
- [19] J. Salmi and A. Molisch, "Propagation parameter estimation, modeling and measurements for ultrawideband MIMO radar," *IEEE Trans. Antennas Propag.*, vol. 59, no. 11, pp. 4257–4267, Nov. 2011.
- [20] D. Shutin, W. Wang, and T. Jost, "Incremental sparse Bayesian learning for parameter estimation of superimposed signals," in *Proc. SampTA-13*, Bremen, Germany, Jul. 2013.
- [21] M. A. Badiu, T. L. Hansen, and B. H. Fleury, "Variational Bayesian inference of line spectra," *IEEE Trans. Signal Process.*, vol. 65, no. 9, pp. 2247–2261, May 2017.
- [22] E. Leitinger, F. Meyer, F. Tufvesson, and K. Witrisal, "Factor graph based simultaneous localization and mapping using multipath channel information," in *Proc. IEEE ICC-17*, Paris, France, Jun. 2017.
- [23] Y. Bar-Shalom and X.-R. Li, *Multitarget-Multisensor Tracking: Principles and Techniques*. Storrs, CT, USA: Yaakov Bar-Shalom, 1995.
- [24] D. Musicki and R. Evans, "Joint integrated probabilistic data association: JIPDA," *IEEE Trans. Aerosp. Electron. Syst.*, vol. 40, no. 3, pp. 1093–1099, Jul. 2004.

- [25] P. Horridge and S. Maskell, "Searching for, initiating and tracking multiple targets using existence probabilities," in *Proc. FUSION-09*, Seattle, WA, USA, Jul. 2009, pp. 611–617.
- [26] —, "Using a probabilistic hypothesis density filter to confirm tracks in a multi-target environment," in *Proc. INFORMATIK-11*, Berlin, Germany, Jul. 2011.
- [27] R. P. S. Mahler, *Statistical Multisource-Multitarget Information Fusion*. Norwood, MA, USA: Artech House, 2007.
- [28] H.-A. Loeliger, "An introduction to factor graphs," *IEEE Signal Process. Mag.*, vol. 21, no. 1, pp. 28–41, Jan. 2004.
- [29] F. Kschischang, B. Frey, and H.-A. Loeliger, "Factor graphs and the sum-product algorithm," *IEEE Trans. Inf. Theory*, vol. 47, no. 2, pp. 498–519, Feb. 2001.
- [30] J. Williams and R. Lau, "Approximate evaluation of marginal association probabilities with belief propagation," *IEEE Trans. Aerosp. Electron. Syst.*, vol. 50, no. 4, pp. 2942–2959, Oct. 2014.
- [31] F. Meyer, P. Braca, P. Willett, and F. Hlawatsch, "A scalable algorithm for tracking an unknown number of targets using multiple sensors," *IEEE Trans. Signal Process.*, vol. 65, no. 13, pp. 3478–3493, Jul. 2017.
- [32] F. Meyer, P. Braca, F. Hlawatsch, M. Micheli, and K. LePage, "Scalable adaptive multitarget tracking using multiple sensors," in *Proc. IEEE GLOBECOM-16*, Washington D.C., USA, Dec. 2016.
- [33] F. Meyer, P. Braca, P. Willett, and F. Hlawatsch, "Tracking an unknown number of targets using multiple sensors: A belief propagation method," in *Proc. FUSION-16*, Heidelberg, Germany, Jul. 2016, pp. 719–726.
- [34] J. L. Williams, "Marginal multi-Bernoulli filters: RFS derivation of MHT, JIPDA, and association-based MeMBer," *IEEE Trans. Aerosp. Electron. Syst.*, vol. 51, no. 3, pp. 1664–1687, Jul. 2015.
- [35] T. Kropfreiter, F. Meyer, and F. Hlawatsch, "Sequential Monte Carlo implementation of the track-oriented marginal multi-Bernoulli/Poisson filter," in *Proc. FUSION-16*, Heidelberg, Germany, Jul. 2016, pp. 972–979.
- [36] E. Leitinger, P. Meissner, C. Rudisser, G. Dumphart, and K. Witrisal, "Evaluation of position-related information in multipath components for indoor positioning," *IEEE J. Sel. Areas Commun.*, vol. 33, no. 11, pp. 2313–2328, Nov. 2015.
- [37] J. G. Proakis and M. Salehi, *Digital Communications*, 5th ed. New York, NY, USA: Prentice-Hall, 2008.
- [38] T. Jost, W. Wang, U. Fiebig, and F. Perez-Fontan, "Detection and tracking of mobile propagation channel paths," *IEEE Trans. Antennas Propag.*, vol. 60, no. 10, pp. 4875–4883, Oct. 2012.
- [39] J. Vermaak, S. J. Godsill, and P. Perez, "Monte Carlo filtering for multi target tracking and data association," *IEEE Trans. Aerosp. Electron. Syst.*, vol. 41, no. 1, pp. 309–332, Jan. 2005.
- [40] S. Kay, *Fundamentals of Statistical Signal Processing: Estimation Theory*. Upper Saddle River, NJ, USA: Prentice Hall, 1993.
- [41] F. Meyer, O. Hlinka, H. Wymeersch, E. Riegler, and F. Hlawatsch, "Distributed localization and tracking of mobile networks including noncooperative objects," *IEEE Trans. Signal Inf. Process. Netw.*, vol. 2, no. 1, pp. 57–71, Mar. 2016.
- [42] D. J. Daley and D. Vere-Jones, *An Introduction to the Theory of Point Processes. Vol. I*, 2nd ed. New York, NY, USA: Springer, 2003.
- [43] X. R. Li and V. P. Jilkov, "Survey of maneuvering target tracking. Part I. Dynamic models," *IEEE Trans. Aerosp. Electron. Syst.*, vol. 39, no. 4, pp. 1333–1364, Oct. 2003.
- [44] D. Schuhmacher, B.-T. Vo, and B.-N. Vo, "A consistent metric for performance evaluation of multi-object filters," *IEEE Trans. Signal Process.*, vol. 56, no. 8, pp. 3447–3457, Aug. 2008.
- [45] P. Meissner, E. Leitinger, and K. Witrisal, "UWB for robust indoor tracking: Weighting of multipath components for efficient estimation," *IEEE Wireless Comm. Lett.*, vol. 3, no. 5, pp. 501–504, Oct. 2014.